みにれびゅう

器官サイズを調節する転写共役因子YAPの活性制御

畠　星治[1,2]，堅田　利明[1]，仁科　博史[2]

1. はじめに

組織における細胞の数の制御は，器官のサイズや組織の恒常性の維持に必須であり，この破綻は器官形成不全や発がんに至る．がん抑制シグナル伝達経路の一つであるHippo経路は，細胞の増殖，生死，分化などを制御して組織における「細胞の数」を調節し，器官のサイズや組織の恒常性を維持している[1]．YAP（yes-associated protein）とそのパラログであるTAZ（transcriptional coactivator with PDZ-binding motif）は，Hippo経路の中心的な役割を果たす転写共役因子である．YAPとTAZはさまざまな遺伝子発現の誘導を介して細胞増殖を促進し細胞死を抑制することでHippo経路のエフェクターとして機能する．近年では多様なHippo経路の上流の制御機構が明らかにされ，細胞が接触する細胞外基質や隣接する細胞との接着といった細胞の接触状態の違いによってHippo経路の活性が巧妙に制御されていることが明らかになりつつある．本稿では，Hippo経路の中心的役割を担うYAPの制御機構に焦点をあて，進展の目覚ましい本領域における最新の知見を哺乳動物に関するものを中心として概説するとともに，我々が最近明らかにした翻訳後修飾を介したYAPの新たな制御機構に関する研究成果を紹介する．

2. YAPによる器官サイズと発がんの制御

器官のサイズは，構成する「細胞の数」と「個々の細胞の大きさ」によって規定されており，Hippo-YAP経路は器官における「細胞数」の制御を担う（図1）．一方，「個々の細胞の大きさ」は栄養状態を感知するmTOR経路により制御されていることが知られているが，多くの場合，器官のサイズ制御は「細胞の数」に依存している[1]．肝臓や心臓などのいくつかの器官においてYAP依存的にサイズが制御されていることが示されており，特に肝臓においては顕著である．マウス肝臓の肝実質細胞においてYAPを過剰発現させると，肝実質細胞の増殖が亢進し，通常は全体重の約5%に維持されている肝臓重量比が約25%にまで増大することが示されている[2]．興味深いことに，肝臓が増大した後にYAPの発現誘導を中止すると，肝臓は元のサイズにまで戻る．これは，肝臓のサイズがYAP依存的に可逆的に制御されていることを示唆している．さらに，長期間にわたってYAPの発現を誘導すると，肝細胞がんの発症に至る．肝細胞がんを含むヒトのさまざまな種類のがん症例において，YAP遺伝子座を含むゲノム領域が増幅しており，YAPの発現量の増加や核内局在の亢進が報告されていることからも，YAPはがん遺伝子産物であることが明らかとなっている[3,4]．

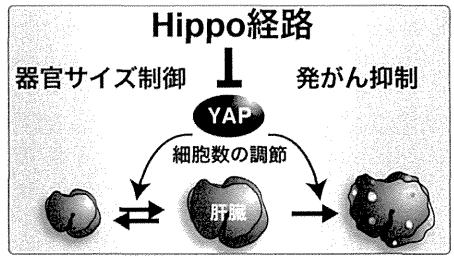

図1　Hippo-YAP経路による器官サイズ制御と発がん抑制

3. Hippo経路によるリン酸化を介したYAPの機能抑制機構

哺乳動物のHippo経路の主要構成因子はショウジョウバエのHippoのホモログであるMst1/2（mammalian ste20-like kinase 1と2），Lats1/2（large tumor suppressor 1と2），Sav（salvador），Mob1（mps one binder 1），YAPとTAZおよびTEAD1/2/3/4である[1]（図2A）．YAPとTAZは転写共役因子であり，転写活性化ドメインを有するもののDNA結合ドメインは持たない．このため，YAPは核内にてさまざまな転写因子と結合することで各々の転写因子が標的

[1] 東京大学大学院薬学系研究科生理化学教室（〒113-0033 東京都文京区本郷7-3-1）
[2] 東京医科歯科大学難治疾患研究所発生再生生物学分野

Regulations of YAP transcriptional co-activator

Shoji Hata[1,2], Toshiaki Katada[1] and Hiroshi Nishina[2]
([1]Laboratory of Physiological Chemistry, Graduate School of Pharmaceutical Sciences, The University of Tokyo, 7-3-1 Hongo, Bukyo-ku, Tokyo 113-0033, Japan; [2]Department of Developmental and Regenerative Biology, Medical Research Institute, Tokyo Medical and Dental University)

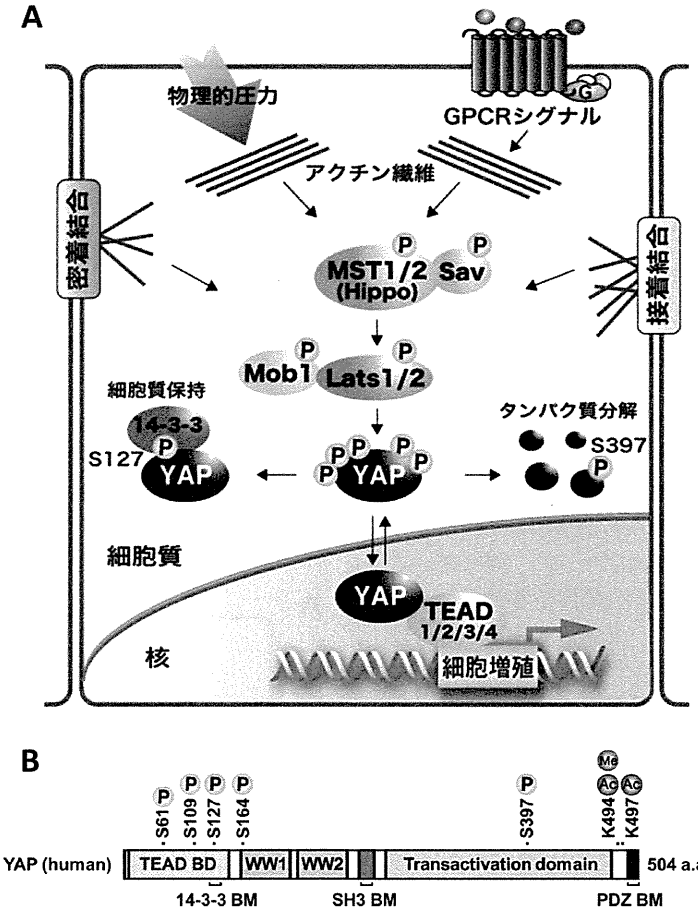

図2　Hippo経路によるYAPのリン酸化制御
（A）Hippo経路の模式図．（B）YAPのドメイン構造．Hippo経路による5か所のリン酸化部位（P）と新たに同定されたアセチル化（Ac）およびモノメチル化部位（Me）．

とする遺伝子の発現を誘導する．中でも，YAPの機能を主に介在する転写因子はTEADであり，TEADは細胞増殖の促進や細胞死の抑制に関与する遺伝子群の発現を担っている．

Hippo経路においてシグナル伝達経路としての中核をなすのは，セリン／トレオニンキナーゼのMst1/2とLats1/2によるキナーゼカスケードである．Mst1/2はLats1/2をリン酸化して活性化させる．活性化されたLats1/2はYAPの5か所のセリン残基をリン酸化する（図2B）．127番目のセリン残基がリン酸化されると，14-3-3タンパク質がこの部位に直接結合することによりYAPを細胞質に保持する[4]．その結果，YAPの核内局在が抑制されてYAP依存的な遺伝子発現が負に制御される．また，YAPの397番目のセリン残基がLats1/2によりリン酸化されると，ユビキチンリガーゼ複合体との相互作用が誘導され，YAPはユビキチン・プロテアソーム系依存的に分解される[5]．このように，Hippo経路はリン酸化を介してYAPの細胞内局在と安定性を制御することで，YAPによる細胞増殖や発がん性形質転換の誘導を抑制している．

Hippo経路の主要構成因子は，ヒトから海綿動物に至る後生動物間において進化的にほぼ保存されている[6]．植物には保存されていないものの，一部の単細胞真核生物にまで保存されている点は興味深い．Hippo経路の起源は出芽酵母における分裂期脱出制御分子群（Mitotic Exit Network）や分裂酵母における隔壁形成分子群（Septation Initiation Network）にあると考えられており，主要構成因子が保存されているだけでなく，シグナル伝達機構も類似している[7]．YAP自体は酵母に保存されていないものの，非後生生物であるアメーバ型の真核単細胞生物*Capsaspora owczarzaki*には保存されている[8]．このYAPホモログも組織サイズ制御能力を保持することがショウジョウバエを用いた解析により示されている．このため，Hippo-YAP経路は進化的に広く保存された細胞の増殖制御機構であるとみなすことができる．

4. 細胞の接触状態を感知するアクチン細胞骨格によるYAPの活性制御

生体器官において血球系以外の細胞は隣接する細胞や周囲の細胞外基質と常に接触した状態にある．細胞による接触状態の感知は組織の恒常性維持に重要であり，その重要性は，非腫瘍性培養細胞株が接触阻害（contact inhibition）という高細胞密度時にみられる増殖停止機構を有することからも示唆される．Hippo経路は細胞間の接触によって活性化され，接触阻害の分子機構として機能することが示されている[4]．特に，上皮細胞はさまざまな細胞間結合によって隣接した細胞と強固に接着している．上皮細胞間結合やそれによって形成される上皮細胞極性の維持は，細胞の腫瘍抑制機構の一つであり，それらが崩壊した細胞ではYAPが活性化していることが示されている[1]．興味深いことに，Hippo経路の上流制御因子として同定されている多くの分子が，密着結合，接着結合，頂端極性複合体の構成因子として知られている．

細胞は隣接した細胞に加えて細胞外基質にも接触しており，このような接触による外的な物理的圧力を感知して，増殖や遊走といったさまざまな細胞の挙動を制御している．アクチンなどの細胞内骨格がこのような物理的圧力の感知を担っているが，そのシグナルがYAPおよびTAZを介して核内での遺伝子発現誘導に至ることが近年明らかになった[9]．接触する細胞外基質の剛性が高いときや細胞の形態が広がっている場合には，接着斑を介して細胞内のアクチン線維の張力が高まり，YAPおよびTAZの活性化を誘導する．アクチン線維からYAPの活性化に至る分子機構は未解明な点が多いが，Hippo経路依存的な機構と非依存的な機構が報告されている．興味深いことに，物理的圧力に加えて，Gタンパク質共役型受容体（GPCR）シグナル伝達経路といった，アクチン線維の形成やストレスファイバーの形成を誘導する刺激もYAPの活性化を誘導することが報告された[10]．また，上皮細胞における接着結合の細胞質側にはアクチン線維が集積しており，密着結合によって形成される上皮細胞極性にはアクチン細胞骨格が必要である．これらのことから，細胞の接触状態に依存したアクチン細胞骨格の変化に応答してYAPの活性化状態を制御し，細胞は増殖や遊走，分化といった細胞機能を発揮していると考えられる．

5. アセチル化とメチル化によるYAPの新たな制御機構

1) アセチル化によるYAPの制御

上記のように，細胞質におけるYAPの制御機構は詳細に解析されているが，YAPが機能する核内での制御機構については不明な点が多い．我々はこの点に着目し，YAPの核内移行を誘導する刺激を利用して核内におけるYAPの制御機構を探索し，YAPが新たにアセチル化されることを見いだした[11]．解析の結果，①YAPのC末端近傍の2か所のリシン残基（K494とK497）がアセチル化修飾を受けること，②YAPのアセチル化が核内に局在するアセチル化酵素CBP/p300によって担われていること，③脱アセチル化を担う酵素はSIRT1であること，④アセチル化部位の変異によりYAPの転写活性化能が変化することを見いだした（図3A）．CBP/p300はYAPと同様に転写共役因子として機能することが知られており，また，SIRT1もエピジェネティックな制御を介して遺伝子発現を調節することが知られている．このため，これらの酵素はYAPのアセチル化状態を制御して，YAPによる遺伝子発現誘

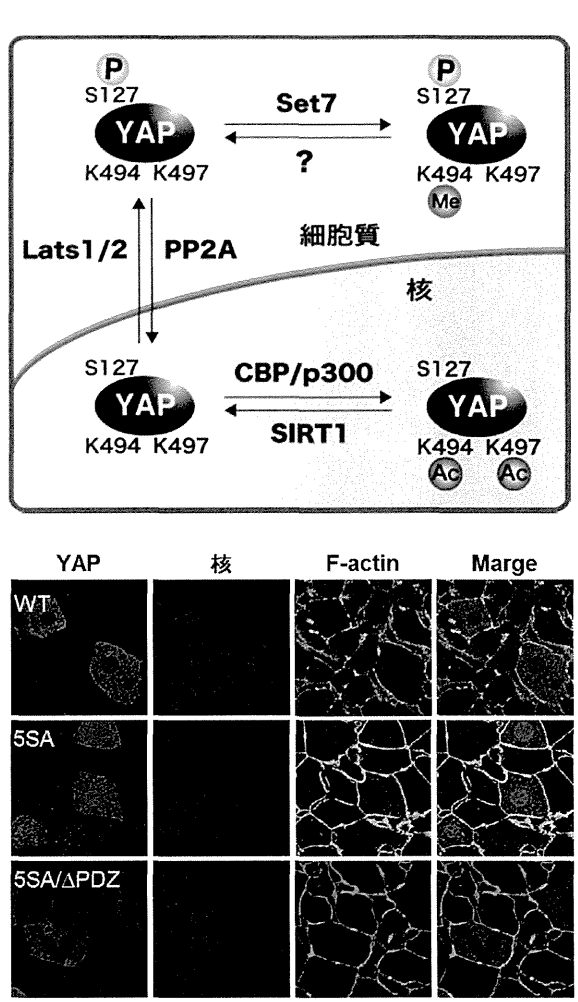

図3　YAPの翻訳後修飾と細胞内局在制御
（A）YAPのリン酸化，アセチル化，モノメチル化修飾と触媒酵素．（B）野生型YAP（上段）と変異型YAP（中，下段）のマウス肝細胞内局在．

導を調節している可能性が考えられる．

2) モノメチル化によるYAPの制御

YAPのアセチル化部位の一つであるK494は，ショウジョウバエからヒトに至るまで進化上高度に保存されているアミノ酸残基である．我々はZaphらのグループとの共同研究により，YAPのK494が新たにモノメチル化されることを明らかにした（図3A）[12]．解析の結果，①メチル化酵素Set7がYAPのモノメチル化および培養線維芽細胞での細胞質への局在化に必要であること，②Set7を欠損したマウスの腸管上皮において前駆細胞の増加を伴う形態異常が生じること，③この前駆細胞ではYAPの核内局在が亢進し下流遺伝子群の発現が亢進することを見いだした．培養線維芽細胞においてSet7は主に細胞質に局在していることから，YAPのモノメチル化は細胞質で生じており，YAPを細胞質に保持するために機能していることが示唆される．また，Set7欠損マウスで観察される表現型はHippo経路の破綻によって生じる表現型と類似している．これらの結果は，リン酸化修飾に加えて，モノメチル化修飾によるYAPの機能制御も個体の組織恒常性維持において重要な役割を担っていることを示唆している．

3) アセチル化／モノメチル化部位の近傍に存在するPDZ-binding motifの機能

YAPのアセチル化／モノメチル化部位であるK494のC末端側の数アミノ酸近傍に，PDZ-BM（PDZ-binding motif）が存在する．我々は最近，このPDZ-BMが生体マウス肝臓の肝実質細胞において，YAPの核内局在に必須であることを見いだした[13]（図3B）．野生型のYAP（WT）は肝実質細胞において細胞質に局在するが，Hippo経路によるリン酸化部位をアラニン残基に変異させたYAP（5SA）は核内に強く局在する．しかし，PDZ-BMを欠失したYAP（5SA/ΔPDZ）は核内に局在することはできない．YAPの細胞内局在を制御する分子の一つとしてPDZドメインを有するZO2（zonula occludens 2）が報告されている[11]．このため，YAPのアセチル化／モノメチル化は近傍のPDZ-BMの機能に影響を与え，ZO2などのPDZドメイン含有タンパク質との相互作用を変化させることでYAPの細胞内局在を制御している可能性が考えられる．

リシン残基はアセチル化修飾とメチル化修飾を同時に受けることができないことから，リシン残基の修飾状態の変化はタンパク質の機能を切り替えるスイッチとして働く可能性がある．これまでに，ヒストンH3のK9がアセチル化とトリメチル化の修飾を受け，これらの修飾がクロマチン構造の変換のスイッチの役割を果たすことが知られている[15]．それゆえ，YAPにおけるK494のアセチル化とモノメチル化もYAPの機能を制御するスイッチとして働き，転写活性化能の調節や細胞内局在制御を担う可能性が考えられる．

6. おわりに

器官のサイズ制御機構は長い間不明であったが，近年の研究の進展により，器官サイズを制御する細胞内の分子機構（Hippo-YAP経路）の実態と，個々の細胞が置かれている状況（情報）を細胞内へ伝達する分子機構（アクチン細胞骨格による接触情報の感知）が明らかとなりつつある．このような知見を基盤として，器官サイズ制御機構においていまだ不明な点の多い，器官レベルと細胞レベルの二つの階層間の隔たりを埋める分子機構の解明が期待される．

1) Yu, F.X. & Guan, K.L. (2013) *Genes Dev.*, 27, 355–371.
2) Dong, J., Feldmann, G., Huang, J., Wu, S., Zhang, N., Comerford, S.A., Gayyed, M.F., Anders, R.A., Maitra, A., & Pan, D. (2007) *Cell*, 130, 1120–1133.
3) Zender, L., Spector, M.S., Xue, W., Flemming, P., Cordon-Cardo, C., Silke, J., Fan, S.T., Luk, J.M., Wigler, M., Hannon, G.J., Mu, D., Lucito, R., Powers, S., & Lowe, S.W. (2006) *Cell*, 125, 1253–1267.
4) Zhao, B., Wei, X., Li, W., Udan, R.S., Yang, Q., Kim, J., Xie, J., Ikenoue, T., Yu, J., Li, L., Zheng, P., Ye, K., Chinnaiyan, A., Halder, G., Lai, Z.C., & Guan, K.L. (2007) *Genes Dev.*, 21, 2747–2761.
5) Zhao, B., Li, L., Tumaneng, K., Wang, C.Y., & Guan, K.L. (2010) *Genes Dev.*, 24, 72–85.
6) Hilman, D. & Gat, U. (2011) *Mol. Biol. Evol.*, 28, 2403–2417.
7) Hergovich, A. & Hemmings, B.A. (2012) *Semin. Cell Dev. Biol.*, 23, 794–802.
8) Sebe-Pedros, A., Zheng, Y., Ruiz-Trillo, I., & Pan, D. (2012) *Cell Rep.*, 1, 13–20.
9) Dupont, S., Morsut, L., Aragona, M., Enzo, E., Giulitti, S., Cordenonsi, M., Zanconato, F., Le Digabel, J., Forcato, M., Bicciato, S., Elvassore, N., & Piccolo, S. (2010) *Nature*, 474, 179–183.
10) Yu, F.X., Zhao, B., Panupinthu, N., Jewell, J.L., Lian, I., Wang, L.H., Zhao, J., Yuan, H., Tumaneng, K., Li, H., Fu, X. D., Mills, G.B., & Guan, K.L. (2012) *Cell*, 150, 780–791.
11) Hata, S., Hirayama, J., Kajiho, H., Nakagawa, K., Hata, Y., Katada, T., Furutani-Seiki, M., & Nishina, H. (2012) *J. Biol. Chem.*, 287, 22089–22098.
12) Oudhoff, M.J., Freeman, S.A., Couzens, A.L., Antignano, F., Kuznetsova, E., Min, P.H., Northrop, J.P., Lehnertz, B., Barsyte-Lovejoy, D., Vedadi, M., Arrowsmith, C.H., Nishina, H., Gold, M.R., Rossi, F.M., Gingras, A.C., & Zaph, C. (2013) *Dev. Cell*, 26, 188–194.
13) Shimomura, T., Miyamura, N., Hata, S., Miura, R., Hirayama, J., & Nishina, H. (2014) *Biochem. Biophys. Res. Commun.*, 443, 917–923.
14) Oka, T., Remue, E., Meerschaert, K., Vanloo, B., Boucherie, C., Gfeller, D., Bader, G.D., Sidhu, S.S., Vandekerckhove, J., Gettemans, J., & Sudol, M. (2010) *Biochem. J.*, 432, 461–472.
15) Sims, R.J., 3rd, Nishioka, K., & Reinberg, D. (2003) *Trends Genet.*, 19, 629–639.

著者寸描

●畠　星治（はた　しょうじ）

日本学術振興会特別研究員（PD），東京大学大学院薬学系研究科生理化学教室所属．理学博士．

■**略歴**　1983年埼玉県に生る．2006年東京薬科大学生命科学部卒業．11年東京医科歯科大学大学院生命情報科学部博士課程修了．08～11年日本学術振興会特別研究員（DC1）．11～13年東京医科歯科大学難治疾患研究所特任助教．13年より現職．

■**研究テーマと抱負**　腫瘍抑制機構の解明をHippo経路の観点から行っている．14年3月からドイツ・ハイデルベルク大学Elmar Schiebel研究室との共同研究のため，長期の渡独．ドイツ留学を楽しみたい．

■**ウェブサイト**　http://www.f.u-tokyo.ac.jp/~seiri/

■**趣味**　料理，ソフトテニス．

肝形成および肝癌における Hippo-YAPシグナル経路の役割

Roles of Hippo-YAP signaling pathway for liver formation and liver cancer

千葉恭敬(写真)　仁科博史
Takanori CHIBA[1,2] and Hiroshi NISHINA[1]
東京医科歯科大学難治疾患研究所発生再生生物学分野[1]，同大学院医歯学総合研究科分子内分泌代謝学分野[2]

◎肝は糖質・蛋白質・脂質などの代謝をはじめ，有害物質の解毒や胆汁酸の生成・分泌など多岐にわたる機能を有しており，生体の恒常性維持に必要不可欠な器官である．そのため生命活動を維持するのに十分な肝機能を発揮できるように，肝はつねに適切な器官サイズ制御を受けている．近年，細胞内情報伝達経路のひとつであるHippoシグナル経路が，転写共役因子であるYAPの活性制御を介してマウスの肝サイズを調節していることが明らかとなった．また，Hippo-YAPシグナル経路は肝癌発症や肝内胆管の発生にも関与することも見出されている．さらに最近では，ヒトの肝癌発症や小児の胆道形成に対するHippo-YAPシグナル経路の関与を示唆する臨床的な知見も数多く報告されている．本稿ではこのような最近の知見を踏まえ，マウスおよびヒトの肝におけるHippo-YAPシグナル経路の役割について紹介する．

Key word：Hippo，YAP，肝サイズ，肝癌，胆管形成

肝は個体の生命維持に必須の器官であり，その機能不全は個体の死に直結する．肝機能不全をきたす代表的な疾患は肝癌(肝細胞癌，胆管細胞癌，肝芽腫など)である．肝癌は，肝を構成する細胞が腫瘍性に増殖することにより発症する．通常，肝を構成する細胞は適切な数を保つように調節されているが，遺伝子変化などにより癌化能力を獲得すると，こうした細胞数の制御から外れ無秩序に増殖し続け，最終的に肝癌を発症する．これまで肝の細胞数を調節するメカニズムは不明であったが，近年になり徐々に解明されつつある．

Hippo-YAPシグナル経路

Hippoシグナル経路はmammalian Ste20-like kinase 1/2(MST1/2)，large tumor suppressor 1/2(LATS1/2)，salvador 1(SAV1)，mps one binder 1a/1b(MOB1A/1B)により構成されており，Hippoシグナル経路は転写共役因子であるYAPをリン酸化することにより負に制御する(図1)．

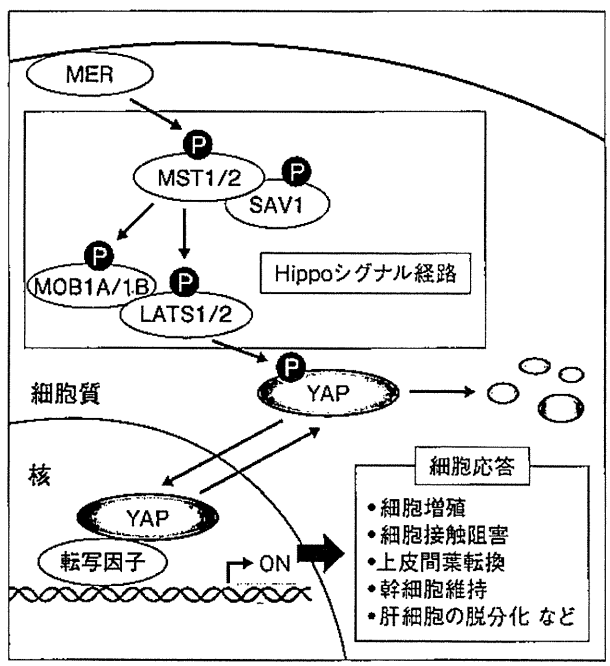

図1　種々の細胞応答を制御するHippo-YAPシグナル経路
MERはHippoシグナル経路の上流分子であり，Hippoシグナル経路はYAPを負に制御する．YAPは種々の細胞応答を引き起こす遺伝子の発現を制御する．

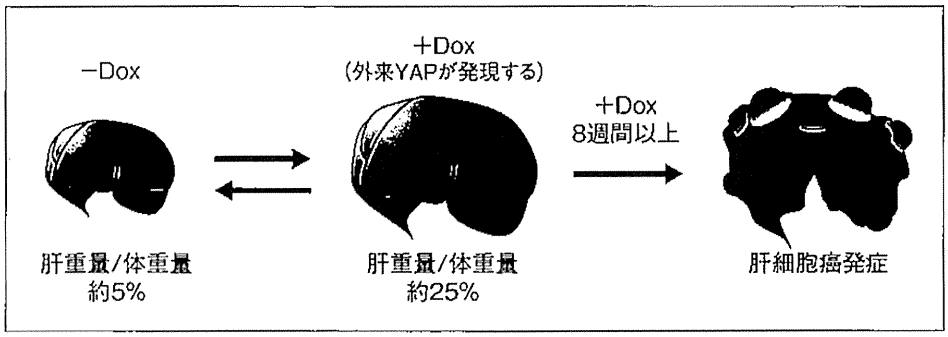

図 2　外来YAP発現誘導による肝のサイズ増大と肝癌発症
Dox 依存的に外来 YAP を過剰発現する Tg マウスの肝．体重に占める肝重量の割合は通常 5%程度であるが，Dox を投与すると約 25%に増加する．しかし，Dox の投与を中止すると肝のサイズは元に戻る．一方，8 週間以上 Dox を持続的に投与すると肝細胞癌が生じる．

Hippo シグナル経路によってリン酸化された YAP は細胞質に保持または分解される．一方，リン酸化を受けていない YAP は活性型として核内で転写因子と結合し，YAP 依存的な遺伝子発現を誘導する．Hippo シグナル経路の代表的な上流分子として，ヒトⅡ型神経線維鞘腫の原因遺伝子として同定された *neurofibromatosis type 2*(*Nf2*)遺伝子がコードする蛋白質 merlin(MER)が知られている．Hippo-YAP シグナル経路は，細胞レベルの機能として細胞増殖，細胞接触阻害(contact inhibition)，上皮間葉転換(epithelial mesenchymal transition)，幹細胞維持，および肝細胞の脱分化などにかかわることが報告されている[1-3]．

Hippo-YAPシグナル経路による成体マウスの肝サイズ制御と発癌抑制

2007 年に Dong らは，ドキシサイクリン(Dox)依存的に肝で YAP を過剰発現するトランスジェニック(Tg)マウスを作出した[4](図 2)．本 Tg マウスにおいて Dox を投与すると，肝のサイズが野生型マウスと比較して約 5 倍にまで増加した．肝のサイズは“細胞の数”と“細胞の大きさ”により規定されるが，本 Tg マウスはおもに“細胞の数”の増加により肝のサイズが増大していることが明らかとなった．興味深いことに，この増大した肝のサイズは Dox 投与を中止すると元に戻る．すなわち，YAP による肝のサイズ制御は可逆的であることが示された．一方，8 週間以上の長期間にわたり Dox を投与し続けた本 Tg マウスは肝細胞癌を発症した．以上の結果から，YAP は“細胞の数”を調節することにより肝のサイズを制御しており，このサイズ制御の長期間にわたる破綻が肝癌を惹起したと考えられる．

2009 年以降には，Hippo シグナル経路の構成分子を肝特異的にノックアウト(KO)したマウスの解析がつぎつぎと報告されてきた(表 1)．MST1 と MST2 の両者の肝特異的な KO マウスは野生型のマウスと比較して生後 2 カ月の段階で肝のサイズが 5 倍程度まで増大し，生後 3〜6 カ月において肝細胞癌を発症することが複数のグループにより示された[5-7]．SAV1 の肝特異的な KO マウスは生後 4 カ月において肝のサイズが 1.5 倍程度に増大し，生後 12〜14 カ月ごろに肝細胞癌や胆管細胞癌を発症する[6,8]．さらに，肝において MOB1A/1B が欠損したマウスは生後 17 カ月ごろに肝癌を発症する[9]．また，Hippo シグナル経路の上流分子である MER の肝特異的な KO マウスは肝のサイズが 5〜7 倍程度に増大し，生後 7〜12 カ月において肝細胞癌や胆管細胞癌を発症する[10,11]．以上のように，Hippo シグナル経路の構成分子や上流分子の KO マウスは YAP Tg マウスと同様に肝のサイズが増大し肝癌を発症することが明らかとなった．

YAPによる発生期のマウス肝形成の制御

マウス肝の発生は胎生 8 日(E8)ごろに，前腸内胚葉に肝の予定領域が決定されることよりはじまる．肝の発生の進行に伴い，肝内胆管の形成が起

表 1　Hippo-YAPシグナル経路構成分子の遺伝子改変マウスの表現型

分子	遺伝子改変マウス	肝のサイズ増大	肝癌形成	文献
MER	*Nf2*$^{+/-}$	−	+	23)
	Alb-Cre Nf2$^{f/f}$	+	+	10,11)
MST1/2	*Mst1*$^{-/-}$*Mst2*$^{+/-}$*1	+	+	5)
	Mst1$^{+/-}$*Mst2*$^{-/-}$*2	+	+	5,24)
	Alb-Cre Mst1$^{-/-}$*Mst2*$^{f/f}$	+	+	5)
	Ad-Cre Mst1$^{-/-}$*Mst2*$^{f/-}$	+	+	5)
	Alb-Cre Mst1$^{f/f}$*Mst2*$^{f/f}$	+	+	6)
	Alb-Cre Mst1$^{-/-}$*Mst2*$^{f/-}$	+	未記載	7)
	CAGGS-CreER Mst1$^{-/-}$*Mst2*$^{f/-}$	+	+	7)
SAV1	*Sav*$^{+/-}$	−	+	8)
	Alb-Cre Sav1$^{f/f}$	+	+	6,8)
	MMTV-Cre Sav1$^{f/f}$	未記載	+	6)
	CAGGS-Cre ER Sav1$^{f/f}$	未記載	+	6)
MOB1A/1B	*Mob1a*$^{\Delta/\Delta}$*Mob1b*$^{tr/+}$*3	未記載	+	9)
YAP	*Tg:ApoE/tTA*	+	+	4)
	Tg:LAP/tTA	+	未記載	25)

*1：Mst2 のアレル欠失が生じると表現型が観察される．
*2：Mst1 のアレル欠失が生じると表現型が観察される．
*3：Mob1b のアレル欠失が生じると表現型が観察される．

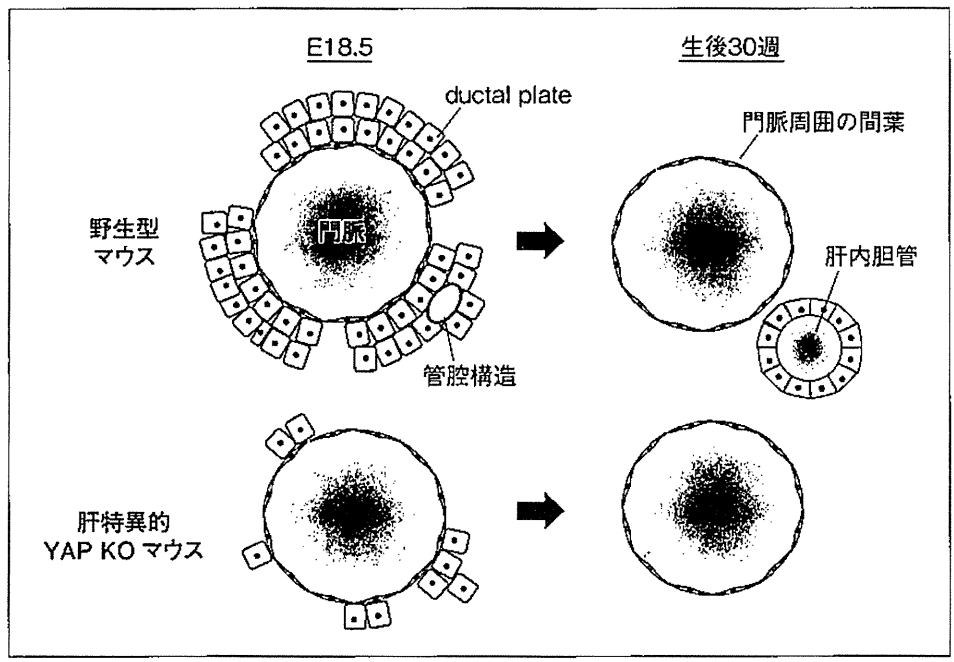

図 3　肝特異的YAP KOマウスにおける肝内胆管発生異常の解析
上：野生型マウスにおける正常な肝内胆管形成過程．E18.5 では ductal plate により管腔構造が形成され，生後 30 週には正常な肝内胆管が形成される．
下：肝特異的 YAP 欠損マウスにおける肝内胆管形成異常．E18.5 では ductal plate の形態異常が生じ，管腔構造ほとんど形成されていなかった．また，生後 30 週では肝内胆管は認めなかった．

こる．肝内胆管の形成過程としては通常，E15.5 ごろに門脈に隣接する胆管前駆細胞から胆管板(ductal plate)が形成され，出生前に ductal plate の一部が管腔構造を呈する．その後，管腔構造は門脈周囲の間葉に取り込まれ肝内胆管となり，残りの ductal plate は生後に退行する．

表 2　ヒト肝癌とHippo-YAPシグナル経路構成分子のかかわり

分子	内容	文献
MST	21 例中 13 例(62%)の肝細胞癌で，切断型 MST1(活性型 MST1)が減少していた	5)
	35 例中 30 例(86%)の肝細胞癌で，リン酸化 MST1(活性型 MST1)が減少していた	13)
LATS	7 例すべての非癌部で LATS は検出されたが，7 例中 4 例(57%)の肝細胞癌で LATS は検出されなかった	14)
MOB1	21 例中 15 例(71%)の肝細胞癌で，リン酸化 MOB1(活性型 MOB1)が減少していた	5)
YAP	*YAP* 遺伝子座を含むゲノム領域(11q22)が増幅されている肝細胞癌を認めた	15)
	33 例の B 型肝炎ウイルス(HBV)陽性患者の肝細胞癌の解析結果では非癌部と比較して癌部の YAP の mRNA 発現は著明に上昇していた．YAP と HBx(HBV がコードする蛋白質)の両 mRNA の発現レベルには正の相関があった	16)
	20 例中 13 例(65%)の肝細胞癌で YAP の発現は亢進していた	4)
	177 例中 110 例(62%)の肝細胞癌で YAP の発現を認め，大部分は YAP は核に存在していた．YAP 陰性と比較して，YAP 陽性肝細胞癌患者は血清 AFP 値が高く，癌の分化度が低かった．また，YAP 陰性と比較して，YAP 陽性肝細胞癌患者の生存率は低かった	17)
	70 例中 47 例(67%)の肝細胞癌では YAP は強く発現していた．予後のよい患者と比較し，予後の悪い患者の肝細胞癌は核局在の YAP や血清 AFP 値の増加を認めた	18)
	115 例中 63 例(54%)の肝細胞癌で，YAP は強く発現していた	19)
	21 例中 7 例(33%)の肝細胞癌で，リン酸化 YAP(不活性型 YAP)は減少していた	5)
	70 例の肝細胞癌，16 例の胆管細胞癌，22 例の肝芽腫の大部分で YAP は核に存在していた	14)
	103 例中 67 例(65%)の肝細胞癌，62 例中 61 例(98%)の胆管細胞癌，94 例中 80 例(85%)の肝芽腫で YAP は核に存在していた	20)
	YAP 陰性と比較して，YAP 陽性肝細胞癌患者は血清 AFP 値が高く，癌の分化度が低かった．また，YAP 陰性と比較して，YAP 陽性肝細胞癌患者の生存率は低かった	21)

発生期の肝形成における YAP の機能に関してはこれまでに全身性 YAP KO マウスが作出されたが，E8.5 ごろに個体の発生が停止してしまうため肝の評価が困難であった[12]．そこで Zhang らは肝特異的に YAP を KO することにより致死を回避することに成功し，胎仔や成体の肝の評価を行った[11]．その結果，本マウスは E18.5 において ductal plate による管腔構造の形成はほとんど認められず，生後30週では正常な肝内胆管は形成されないことが示された(図 3)．また，本マウスの成体は血清ビリルビン値や alanine aminotransferase(ALT)値が上昇しており，さらに肝の線維化をきたしていた．以上のことから，YAP はマウスの肝内胆管の形成に必要であることが明らかとなった．

Hippo-YAPシグナル経路による ヒト肝癌発症とヒト胆道形成の制御

近年，マウスの知見と同様に，ヒトにおいても肝癌発症に Hippo-YAP シグナル経路が関与していることが明らかにされている(表 2)．Hippo-YAP シグナル経路が肝癌発症に関与する際には，肝癌細胞において Hippo シグナル経路が不活性化されている，あるいは YAP が活性化されていると考えられる．ヒト肝癌における Hippo シグナル経路の不活性化については，これまでに MST，LATS，ならびに MOB1 に関する報告がなされている．たとえば，MST に関しては 21 例中 13 例(62%)および 35 例中 30 例(86%)のヒト肝細胞癌では非癌部と比較して活性型 MST1 が減少していることが示された[5,13]．また，LATS に関しては 7 例中 4 例(57%)のヒト肝癌において LATS 蛋白質が検出されないことが報告されている[14]．さらに MOB に関しては，21 例中 15 例(71%)のヒト肝細胞癌では非癌部と比較して活性型 MOB1 が減少していることが示されている[5]．

2006 年にはヒト肝細胞癌において *YAP* 遺伝子座を含むゲノム領域(11q22)が増幅されていることが報告され，YAP がヒト肝細胞癌発症に関与することが示唆された[15]．以降，今日までにヒト肝癌と YAP に関する報告はつぎつぎとなされており，ヒト肝細胞癌では非癌部と比較して YAP

のmRNAや蛋白質の発現レベルが亢進していることが示された[4,16-19]．さらに，ヒト肝細胞癌ではリン酸化を受けた不活性型のYAPが減少していることや，ヒト肝細胞癌，胆管細胞癌，および肝芽腫ではYAPは活性型として，おもに核に存在していることも示された[5,14,17,19,20]．このようにヒト肝癌においてYAPの発現，活性，ならびに核局在の割合が亢進していることが明らかとなってきている．

また，ヒト肝細胞癌の分化度や肝細胞癌患者の血清α-fetoprotein(AFP)値および予後に関する興味深い報告がある．Xuらは，YAP陰性の患者と比較してYAP陽性の肝細胞癌患者は血清AFP値が高いことや癌の分化度が低いことを示した[17]．さらに，YAP陽性の肝細胞癌患者では生存率が有意に低く，5年生存率はYAP陰性の患者は58%であるのに対し，YAP陽性の患者は36%に減少することも報告した．同様にHanらも，YAP陰性の患者と比較して，YAP陽性の肝細胞癌患者では血清AFP値が高いこと，癌の分化度が低いこと，生存率が低いことを示した[21]．以上のように，ヒト肝癌においてもHippo-YAPシグナル経路は肝癌発症の一因を担っていること，YAPは予後マーカーとなることが示唆された．

一方，ヒト胆道の形成とYAPに関する報告もなされている．胆道閉鎖症(BA)は新生児期から乳児期早期に発症する胆汁うっ滞性疾患のひとつであり，胆管の閉塞により重篤な肝障害を引き起こし，早期診断・早期治療が行われなければ死に至る疾患である．2014年にGurdaらはBA以外の原因による胆汁うっ滞性疾患の患児との比較解析によりBAの患児の肝組織では胆管上皮細胞のYAP発現が有意に亢進していることを見出した[22]．これにより，小児の胆汁うっ滞性疾患の鑑別診断を行うにあたりYAPがBAの診断の補助として有用であることが示された．

おわりに

2003年にショウジョウバエにおいて器官サイズを制御するシグナル伝達経路として，Hippo-YAPシグナル経路が同定された．その後10年の間に，マウスを用いた解析によりHippo-YAPシグナル経路の多様な役割が明らかにされてきた．近年ではヒトにおいても，肝癌のみならず卵巣癌や前立腺癌などでHippo-YAPシグナル経路が破綻していることが報告されている[1]．わが国では1981年以降，悪性新生物は死因の第一位であり，その死亡率は増加の一途をたどっている．そのため，今後はHippo-YAPシグナル経路の分子機構の知見を診断や治療に結びつけ，新規癌治療薬開発などが行われていくことが期待される．

謝辞：今回の執筆にあたり多大なご協力をいただいた東京医科歯科大学大学院医歯学総合研究科分子内分泌代謝学分野の小川佳宏先生に深く感謝致します．

文献

1) Harvey, K. F. et al.: *Nat. Rev. Cancer*, **13**: 246-257, 2013.
2) Zhao, B. et al.: *Nat. Cell. Biol.*, **13**: 877-883, 2011.
3) Yimlamai, D. et al.: *Cell*, **157**: 1324-1338, 2014.
4) Dong, J. et al.: *Cell*, **130**: 1120-1133, 2007.
5) Zhou, D. et al.: *Cancer Cell*, **16**: 425-438, 2009.
6) Lu, L. et al.: *Proc. Natl. Acad. Sci. USA*, **107**: 1437-1442, 2010.
7) Song, H. et al.: *Proc. Natl. Acad. Sci. USA*, **107**: 1431-1436, 2010.
8) Lee, K. P. et al.: *Proc. Natl. Acad. Sci. USA*, **107**: 8248-8253, 2010.
9) Nishio, M. et al.: *J. Clin. Invest.*, **112**: 4505-4518, 2012.
10) Benhamouche, S. et al.: *Genes. Dev.*, **24**: 1718-1730, 2010.
11) Zhang, N. et al.: *Dev. Cell*, **19**: 27-38, 2010.
12) Morin-Kensicki, E. M. et al.: *Mol. Cell. Biol.*, **26**: 77-87, 2006.
13) Diego. et al.: *Gastroenterology*, **130**: 1117-1128, 2006.
14) Li, H. et al.: *Liver Int.*, **32**: 38-47, 2012.
15) Zender, L. et al.: *Cell*, **125**: 1253-1267, 2006.
16) Zhang, T. et al.: *Hepatology*, **56**: 2051-2059, 2012.
17) Xu, M. Z. et al.: *Cancer*, **115**: 4576-4585, 2009.
18) Felix, D. et al.: *Gastroenterology*, **144**: 1530-1542, 2013.
19) Zhao, B. et al.: *Genes Dev.*, **21**: 2747-2761, 2007.
20) Tao, J. et al.: *Gastroenterology*, 2014, May 14.(Epub ahead of print)
21) Han, S. X. et al.: *J. Immunol. Res.*, 2014, Apr. 22.(Epub ahead of print)
22) Gurda, G. T. et al.: *Hum. Pathol.*, **45**: 1057-1064, 2014.
23) McClatchey, A. I. et al.: *Genes Dev.*, **12**: 1121-1133, 1998.
24) Avruch, J. et al.: *Br. J. Cancer*, **104**: 24-32, 2011.
25) Camargo, F. D. et al.: *Curr. Biol.*, **17**: 2054-2060, 2007.

J. Biochem. 2014;155(4):235–241 doi:10.1093/jb/mvt114

JB THE JOURNAL OF BIOCHEMISTRY

Overexpression of autotaxin, a lysophosphatidic acid-producing enzyme, enhances cardia bifida induced by hypo-sphingosine-1-phosphate signaling in zebrafish embryo

Received September 30, 2013; accepted December 16, 2013; published online January 21, 2014

Keita Nakanaga[1], Kotaro Hama[1], Kuniyuki Kano[1], Takanao Sato[2], Hiroshi Yukiura[1], Asuka Inoue[1,3], Daisuke Saigusa[4], Hidetoshi Tokuyama[2], Yoshihisa Tomioka[4], Hiroshi Nishina[5], Atsuo Kawahara[6] and Junken Aoki[1,7,*]

[1]Department of Molecular and Cellular Biochemistry, Graduate School of Pharmaceutical Sciences, Tohoku University, 6-3, Aoba, Aramaki, Aoba-ku, Sendai, Miyagi 980-8578, Japan; [2]Laboratory of Medicinal Chemistry, Graduate School of Pharmaceutical Sciences, Tohoku University, 6-3, Aoba, Aramaki, Aoba-ku, Sendai, Miyagi 980-8578, Japan; [3]Presto, JST, 4-1-8 Honcho Kawaguchi, Saitama 332-0012, Japan; [4]Laboratory of Oncology, Pharmacy Practice and Sciences, Graduate School of Pharmaceutical Sciences, Tohoku University, 6-3, Aoba, Aramaki, Aoba-ku, Sendai, Miyagi 980-8578, Japan; [5]Medical Research Institute, Tokyo Medical and Dental University, 1-5-45 Yushima, Bunkyo-ku, Tokyo 113-8510, Japan; [6]Laboratory for Cardiovascular Molecular Dynamics, Riken Quantitative Biology Center, Furuedai 6-2-3, Suita Osaka 565-0874, Japan; and [7]CREST, JST, 4-1-8 Honcho Kawaguchi, Saitama 332-0012, Japan

*Junken Aoki, Department of Molecular and Cellular Biochemistry, Graduate School of Pharmaceutical Sciences, Tohoku University, 6-3, Aoba, Aramaki, Aoba-ku, Sendai, Miyagi 980-8578, Japan. Tel: 81-22-795-6860, Fax: 81-22-795-6859, email: jaoki@m.tohoku.ac.jp

Lysophosphatidic acid (LPA) and sphingosine-1-phosphate (S1P) are second-generation lysophospholipid mediators that exert multiple biological functions through their own cognate receptors. They are both present in the blood stream, activate receptors with similar structures (endothelial differentiation gene receptors), have similar roles in the vasculature and are vasoactive. However, it is unclear whether these lysophospholipid mediators cross-talk downstream of each receptor. Here, we provide *in vivo* evidence that LPA signaling counteracted S1P signaling. When autotaxin (Atx), an LPA-producing enzyme, was overexpressed in zebrafish embryos by injecting *atx* mRNA, the embryos showed cardia bifida, a phenotype induced by down-regulation of S1P signaling. A similar cardiac phenotype was not induced when catalytically inactive Atx was introduced. The cardiac phenotype was synergistically enhanced when antisense morpholino oligonucleotides (MO) against S1P receptor (*s1pr2/mil*) or S1P transporter (*spns2*) was introduced together with *atx* mRNA. The Atx-induced cardia bifida was prominently suppressed when embryos were treated with an *lpar1* receptor antagonist, Ki16425, or with MO against *lpar1*. These results provide the first *in vivo* evidence of cross-talk between LPA and S1P signaling.

Keywords: lysophosphatidic acid/sphingosine-1-phosphate/autotoxin/zebrafish/cardia bifida.

Abbreviations: Atx, autotaxin; *cmlc2*, cardiac myosin light chain 2; Edg, endothelial differentiation gene; hpf, hours post fertilization; LPA, lysophosphatidic acid; LPC, lysophosphatidylcholine; MO, antisense morpholino oligonucleotides; ROCK, Rho kinase; S1P, sphingosine-1-phosphate.

Lysophosphatidic acid (LPA) and sphingosine-1-phosphate (S1P) are lysophospholipid mediators with a number of similar characters. First, the structures of LPA and S1P are quite similar. Second, they are both present in various biological fluids such as plasma, serum and cerebrospinal fluids (*1–4*). Third, they share similar receptors: three LPA receptors (LPA_{1-3}) and all five S1P receptors ($S1P_{1-5}$) belong to the endothelial differentiation gene (Edg) family and share ~35% sequence similarity with each other, although LPA has an additional three receptors belonging to the P2Y family (*5*). Fourth, they have several similar functions that have been demonstrated both *in vivo* and *in vitro*. They both stimulate cell proliferation and motility of various cell types (*6*). They also have critical roles in the vasculature (*7–9*) and are vasoactive (*10*, *11*). Indeed, LPA and S1P regulate blood pressure, both positively and negatively (*12*, *13*). Thus, LPA and S1P appear to share common features and have similar biological roles. However, it is unclear whether there is an interaction between LPA and S1P signaling. Genes involved in LPA and S1P signaling including receptors, producing enzymes, degrading-enzymes and transporters are highly conserved in vertebrates. For example, zebrafish and mammalian autotaxin (Atx) have ~65% amino-acid identity and have similar biochemical and biological roles (*14*). Recent studies of zebrafish and mouse mutants revealed the essential cardiovascular functions of S1P signaling through the S1P transporter *spns2* are conserved from fishes to mammals (*15–19*). These studies have indicated that zebrafish is a useful model organism for elucidating LPA and S1P functions. It may be possible to examine the interaction between LPA signaling and S1P signaling in zebrafish embryos by manipulating the expressions of several genes simultaneously. In this study, we investigated the functional interaction between LPA signaling and S1P signaling by manipulating LPA- and S1P-related genes in zebrafish. Here, we describe the first *in vivo*

evidence showing that LPA signaling affects S1P signaling.

Materials and Methods

Maintenance of zebrafish and drug treatment

Wild-type strain (AB, TU) and transgenic (*cmlc2:mRFP*) were obtained from the Zebrafish International Resource Center (University of Oregon, Eugene, OR) and National BioResource Project, Zebrafish (Riken Brain Research Institute, Wako, Japan). Fish were maintained at 27–28°C under a controlled 13.5-h light/10.5-h dark cycle. Embryos were obtained from natural spawnings and staged according to morphology as described (*20*). Ki16425 was diluted in embryo media supplemented with 1% DMSO and added to zebrafish embryos between 12-h post-fertilization (hpf) and 24 hpf.

mRNA and morpholino injection

The sequences of antisense morpholino oligonucleotides (MO) (Gene Tools, LLC, Corvallis, OR) were designed as previously described (*14*, *16*, *21*). The mRNAs for zebrafish wild-type *atx*, catalytically inactive *atx* (T205A) and mouse wild-type *atx* were synthesized using mMESSAGE MACHINE kit (Ambion, Austin, TX). Morpholinos and synthetic mRNAs were dissolved in water with 0.2% phenol red. Synthetic mRNAs were injected into the blastomere of one cell stage embryos. Morpholinos were injected into the yolk of 1–8 cell stage embryos.

Whole-mount in situ hybridization

An antisense RNA probe labeled with digoxigenin for *cmlc2* was prepared with an RNA labeling kit (Roche Applied Science, Penzberg, Germany). Whole-mount *in situ* hybridization was performed as previously described (*22*).

Evaluation of LPA receptor activation

Activation of LPA receptor was evaluated by a transforming growth factor-α (TGFα) shedding assay as described previously (*23*, *24*). Briefly, each zebrafish LPA receptor gene was introduced into HEK 293T cells together with DNA encoding TGFα fused to alkaline phosphatase. Upon the addition of a ligand for LPA receptors, the TGFα proform expressed on the plasma membrane was cleaved by tumour necrosis factor α converting enzyme (TACE) proteases endogenously expressed in HEK293T cell and thereby released into the culture medium. Then, the activation of LPA receptor was evaluated by measuring the alkaline phosphatase activity in the conditioned medium of the cells.

Measurement of lysophospholipase D activity and Western blotting

Twenty-eight hours after injection, embryos were deyolked as described previously (*14*) and homogenized in lysis buffer [10 mM Tris-HCl (pH 7.4), 10% Triton X-100, 10 μg/ml PMSF, 50 μg/ml Leupeptin, 50 μg/ml Aprotinin] using an ultrasonic homogenizer (Smurt NR-50M; Microtec Nition, Funabashi, Japan). The homogenate was sequentially centrifuged at 21,500 × *g* and the resulting supernatant was collected. Protein concentration was measured with BCA Protein Assay Reagent (Thermo, Waltham, MA) and 5 μg of protein was used for each of lysophospholipase D assay and Western blotting. Lysophospholipase D activity was measured as described previously (*25*). Briefly, the extracts were mixed with 14:0 lysophosphatidylcholine (LPC) (100 mM Tris-HCl, 5 mM $MgCl_2$, 500 mM NaCl, 0.05% Triton X-100, pH 9.0) and incubated for 66 h at 37°C. Liberated choline was quantified using choline oxidase (Wako, Osaka, Japan), peroxidase (TOYOBO, Osaka, Japan) and TOOS reagent (Dojindo, Kumamoto, Japan). The activity was indicated by the generation rate of choline per unit time and protein mass (pmol/μg/h). Western blotting was performed using anti-zebrafish Atx rat polyclonal antibody that was generated as previously described (*14*). Proteins bound to the antibody were visualized with an enhanced chemiluminescence kit (GE Healthcare, Waukesha, WI).

Microscopic analysis and live imaging

Embryos were positioned in 3% methylcellulose (Sigma) on slide glass. Images were captured with a Leica M80 stereomicroscope equipped with Leica DFC425 digital camera (Leica Microsystems, Wetzlar, Germany).

Results

Overexpression of Atx enhances the cardia bifida phenotype in zebrafish embryos

We previously showed that down-regulation of Atx in zebrafish embryos resulted in malformation of the vasculature (*14*). When we tried to rescue the phenotype by injecting mRNA encoding zebrafish *atx* in the embryos, we accidentally found that introduction of *atx* mRNA resulted in an abnormal heart formation (Supplementary movies S1 and S2). Compared with control embryos, blood flow and heart beating were severely impaired at 36 hpf. This phenotype is known as a two-heart or cardia bifida phenotype. In addition, at 54 hpf the tail region of the embryos frequently had blisters (Fig. 1E and F). These are the most characterized phenotypes in previous studies when S1P signal via either S1P receptor (*s1pr2/mil*) or S1P transporter (*spns2*) is attenuated (*15–17*). To examine the cardia bifida phenotype in more detail, we visualized cardiomyocytes by whole-mount *in situ* hybridization using

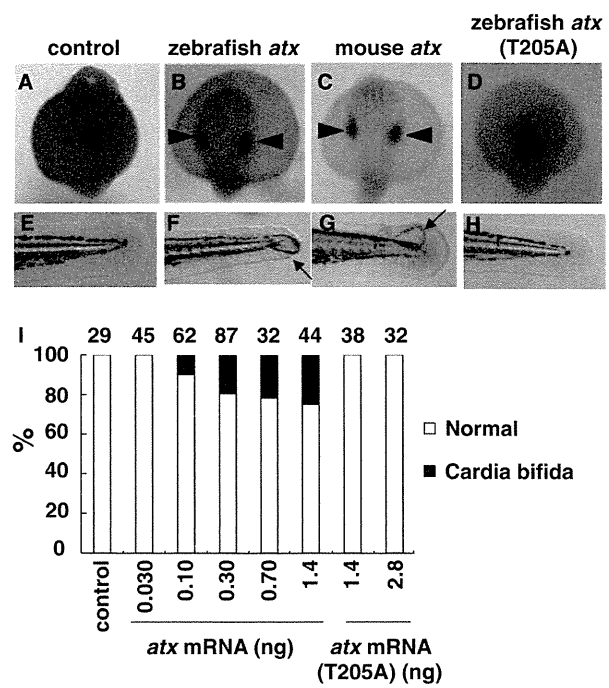

Fig. 1 Overexpression of Atx causes cardia bifida phenotype and tail blisters in zebrafish. Effect of Atx overexpression on the heart formation was examined by whole-mount *in situ* hybridization using *cmlc2* probe (A–D). The phenotypes of cardia bifida (arrowheads) at 24 hpf and tail blister (arrows) at 54 hpf were observed in embryos injected with either wild-type zebrafish *atx* mRNA (B, F) or mouse *atx* mRNA (C, G), which was not observed for catalytically inactive zebrafish *atx* (T205A) mRNA (D, H). (I) Percentage of embryos with cardia bifida phenotype. The number of tested embryos and the amount of mRNA per embryo are listed above and below the graph, respectively. Figures were selected as representative data from three independent experiments.

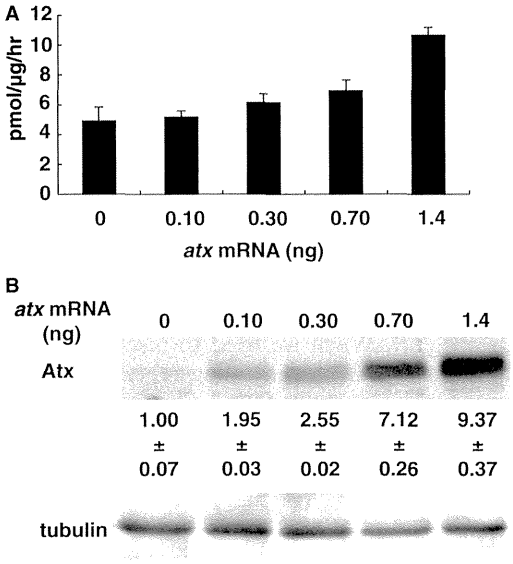

Fig. 2 Expression of Atx in zebrafish embryos injected with *atx* mRNA. Atx enzymatic activity (A) and protein (B) in embryos injected with *atx* mRNA were examined. The enzymatic activity and the protein levels were analyzed by measuring the lysophospholipase D activity in the total lysate of the embryos using LPC as a substrate and Western blot analysis using zebrafish Atx-specific antibody, respectively. The intensity of the bands was determined by densitometrical analysis and the results were shown as the mean ± standard derivation of Atx/tubulin ratios (arbitrary units, $n = 3$).

cardiac myosin light chain 2 (*cmlc2*) probe. At 24 hpf, in control embryos, cardiomyocytes were detected in one cluster in the center of the embryos, whereas two clusters of cardiomyocyte were detected in *atx* mRNA-treated embryos (Fig. 1A and B). Similar cardia bifida and tail blister phenotypes were also observed in embryos treated with mouse *atx* mRNA (Fig. 1C and G). Both lysophospholipase D activity and zebrafish Atx protein increased with the dose of injected *atx* mRNA (Fig. 2A and B) and the phenotype was observed when *atx* mRNA higher than 0.03 ng was employed (Fig. 1I). The cardia bifida phenotype required catalytic activity of Atx because either the cardia bifida phenotype or tail blister phenotype was not induced when mRNA for catalytically inactive zebrafish *atx* (T205A) was injected (Fig. 1D, H and I), suggesting that the cardia bifida phenotype was induced via the product of Atx, that is LPA.

Down-regulation of S1P signaling enhances the Atx-induced cardia bifida phenotype

To address the possible link between S1P and LPA signaling, we examined the Atx-induced cardia bifida phenotype when S1P signal was attenuated. We injected *atx* mRNA simultaneously with *mil* or *spns2* MO. First we injected MO for either *mil* or *spns2* and confirmed that significant cardia bifida phenotype was induced at MO concentrations 3.2 ng or more (*mil*), and 5.0 ng or more (*spns2*), but rarely observed at MO concentrations lower than these dosages (Fig. 3A–E and K). Intriguingly, injection of a low dosage of *mil* (1.6 ng) or *spns2* (1.0 ng) MO with *atx* mRNA (0.1 ng) induced an even more severe bifida phenotype (Fig. 3F, G, I, L and M). Indeed, only 7.0% and 3.0% of embryos displayed the cardia bifida phenotype in *mil* and *spns2* MO-treated embryos, respectively, whereas 90% and 60% of embryos displayed the phenotype when *atx* mRNA was co-injected. We observed that the tail blister phenotype was also synergistically induced when *atx* mRNA was co-injected (data not shown). This synergistic effect by *atx* mRNA was catalytically dependent since mRNA for catalytically inactive zebrafish *atx* (T205A) did not show such effect (Fig. 3H, J and N).

LPA_1 mediates Atx-induced cardia bifida

To confirm the involvement of LPA signaling in Atx-induced cardia bifida, we next tried to identify the LPA receptor mediating the Atx-induced cardia bifida. Addition of a LPA_{1-3} antagonist Ki16425 in embryo medium, which also worked on zebrafish Lpar1–3 (*14*), significantly decreased the occurrence frequency of the cardia bifida phenotype induced by injecting *atx* mRNA and *mil* MO in a dose-dependent manner (Fig. 4A). We recently showed that (*R*)-Ki16425 was more potent in antagonizing mammalian LPA_{1-3} than (*S*)-Ki16425 (*26*). We also confirmed that this is also true for zebrafish Lpar1–3 (Fig. 5). Consistent with this, the cardia bifida phenotype was effectively rescued by (*R*)-Ki16425, but not by (*S*)-Ki16425 (Fig. 4B). We further confirmed that the *lpar1* MO partially rescued the cardia bifida phenotype induced by co-injection of *atx* mRNA and *mil* MO (Fig. 4C). The rescue was not observed with *lpar2–6* MO (data not shown). Together, these findings indicate that the cardia bifida phenotype induced by Atx overexpression in zebrafish embryos is mediated by overproduction of LPA and consequent activation of mainly Lpar1. Thus, these results showed that *atx* mRNA treatment affected cardiomyocyte migration that is regulated by S1P signaling in zebrafish embryos at least through Lpar1.

Discussion

In this study, we found that excess LPA signal in zebrafish embryos led to cardia bifida (two heart) phenotype. Because the same phenotype was induced when S1P signaling was down-regulated, we explored the functional interaction between LPA and S1P signaling in the zebrafish heart morphogenesis and found that LPA signaling down-regulated the S1P signaling that led to the cardia bifida phenotype. To our knowledge, this is the first to demonstrate the functional interaction between LPA and S1P signaling.

Among various LPA receptors Lpar1 appeared to be involved in the LPA-induced cardia bifida phenotype. First, the cardia bifida phenotype induced by the co-administration of *atx* mRNA and *mil* MO was almost completely rescued by Ki16425 (Fig. 4A and B), which were found to antagonize all Edg LPA receptors in zebrafish including Lpar1, Lpar2a, Lpar2b and Lpar3 (Fig. 5). Unlike *lpar2a, lpar2b* and *lpar3*, down-regulation of *lpar1* alone rescued the cardia bifida phenotype, showing that Lpar1 is the major LPA receptor involved. Second, we speculate that the functional interaction between LPA and S1P signaling occurs downstream of

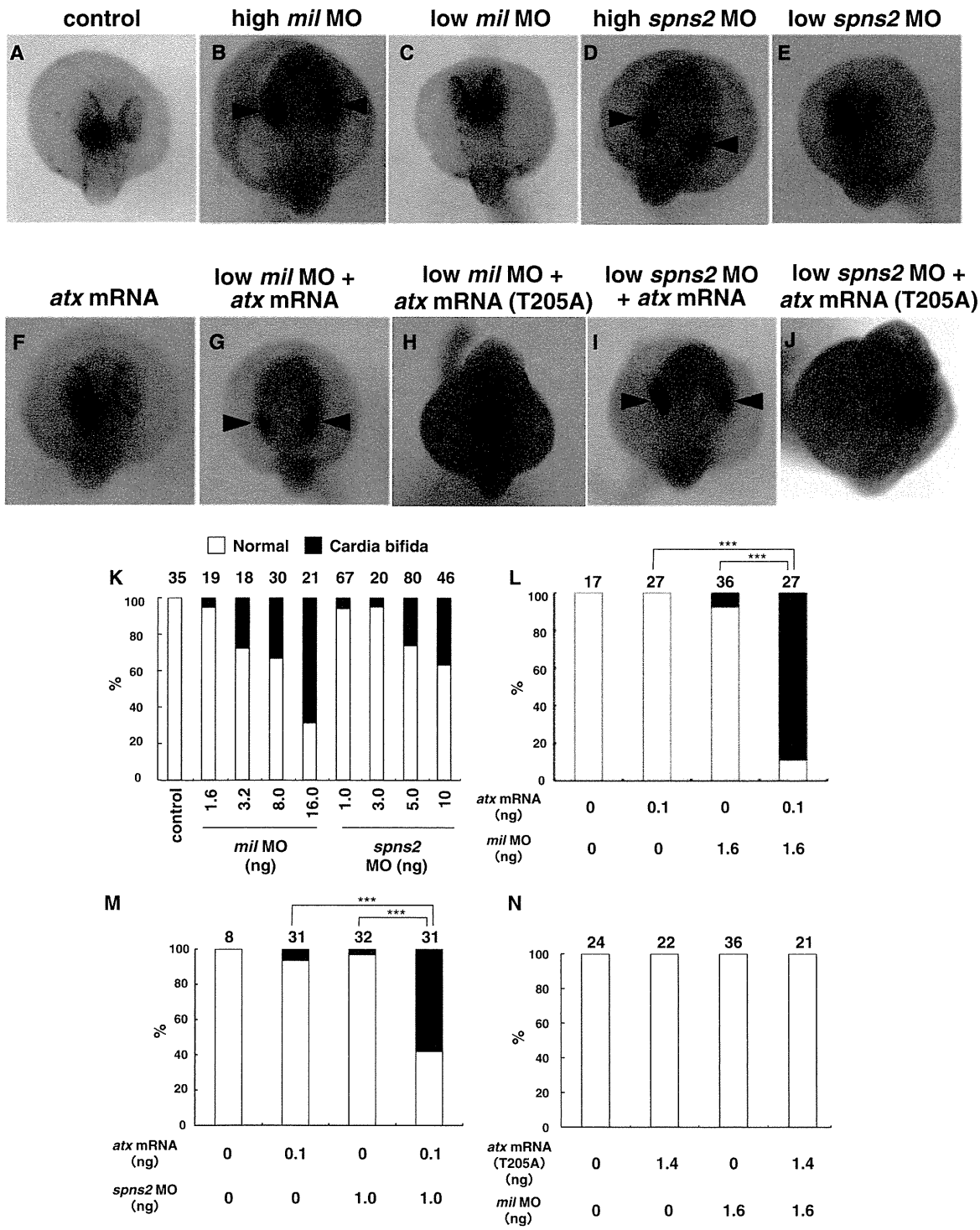

Fig. 3 Cardia bifida phenotype induced by overexpression of Atx was dramatically enhanced when S1P signaling was attenuated. Effect of *mil* and *spns2* down-regulation on cardia bifida phenotype induced by overexpression of Atx was examined. The cardia bifida phenotype was evaluated by whole-mount *in situ* hybridization using *cmlc2* probe at 24 hpf. Cardia bifida phenotype was induced at high concentration of *mil* (8.0 ng) or *spns2* (5.0 ng) MO (B, D). Low *mil* (1.6 ng), low *spns2* (1.0 ng) MO and low *atx* mRNA rarely induced cardia bifida phenotype (C, E, F), whereas co-injection of low *mil* or *spns2* together with *atx* mRNA induced significant cardia bifida phenotype (G, I). These synergistic effects were not observed when catalytically inactive *atx* (T205A) mRNA was co-injected (H, J). (K–N) Percentage of embryos with cardia bifida phenotype was shown. The number of tested embryos, and types of mRNA and MO injected were listed above and below the graph, respectively. K. Dose-dependent increase in the occurrence frequency of the cardia bifida phenotype showing that the phenotype was rarely induced at low dose of MO [1.6 ng (*mil*) and 1.0 ng (*spns2*)]. (L, M) Effect of S1P signal down-regulation on Atx-induced cardia bifida phenotype. Down-regulation of S1P signal was induced either by injecting MO for *mil* (L) or *spns2* (M). Percentage of embryos with cardia bifida phenotype was dramatically increased when *atx* mRNA was injected with MO for *mil* (L) or *spns2* (M) (***$P<0.001$ by χ^2-test). (N) The synergistic effect of *atx* mRNA and S1P-related genes (*mil* and *spns2*) requires catalytic activity of *atx* as catalytically inactive *atx* mRNA did not show the synergistic effect. Figures were selected as representative data from three independent experiments.

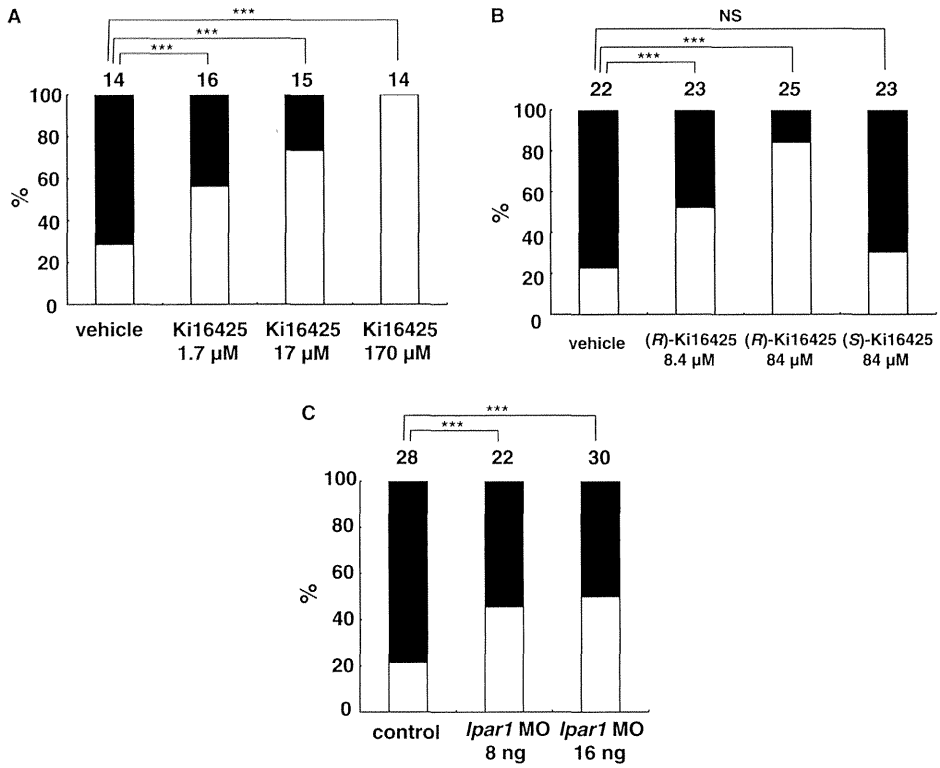

Fig. 4 Cardia bifida phenotype induced by Atx overexpression was mainly mediated by Lpar1. (A, B) Effect of Ki16425 on Atx-induced cardia bifida phenotype in embryos injected with *atx* mRNA (0.1 ng) and *mil* MO (1.6 ng). Ki16425 attenuated cardia bifida phenotype in dose-dependent (A) and enantio-selective (B) manners. (C) Cardia bifida was also recovered by injection of *lpar1* MO (***$P<0.001$ by χ^2-test). NS, not significantly different between the two ($P>0.05$). The number of tested embryos was listed above the graph. Figures were selected as representative data from three independent experiments.

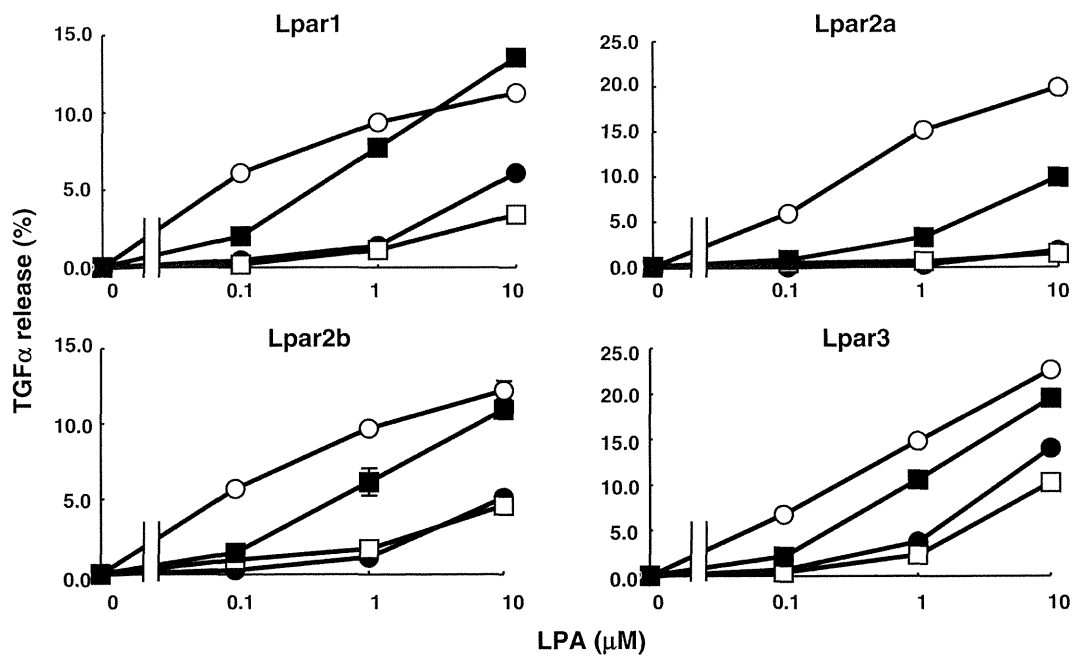

Fig. 5 (*R*)-Ki16425 is potent in antagonizing zebrafish LPA receptors. Activation of the four zebrafish Edg LPA receptors was evaluated by a TGFα shedding assay, in which the activation of each receptor is transduced into TGFα ectodomain shedding. Briefly, HEK293T cells were transfected with cDNAs for each LPA receptor (Lpar1, Lpar2a, Lpar2b and Lpar3), and the amount of alkaline phosphatase (AP)-tagged TGFα released upon LPA stimulation in the presence or absence (open circle) of Ki16425 compounds was determined by measuring AP activity of the culture cell supernatant. (*R*)-Ki16425 (open square) was more potent in antagonizing each LPA receptor than (*S*)-Ki16425 (closed square). The activity of racemic Ki16425 [(*RS*)-Ki16425, closed circle] was also shown. Data represent the means ± standard derivation of triplicate values and are representative of three independent experiments.

each LPA (*lpar1*) and S1P (*mil*) receptor. *Mil* is the zebrafish ortholog of mammalian *s1pr2*. A body of evidence showed that LPA_1 mainly activates $G\alpha_i$-Rac1 signaling whereas $S1P_2$ mainly activates $G\alpha_{12/13}$-RhoA signaling (*5*, *27*). Interestingly, $G\alpha_i$-Tiam1-Rac1 pathway downstream of LPA_1 was shown to inhibit $G\alpha_{12/13}$-mediated RhoA activation in various cell types (*28–30*). Moreover, RhoA and its downstream effector Rho kinase (ROCK) were shown to be essential in cardiac cell migration in both mice and zebrafish (*31*, *32*). Thus, excess Rac1 activation downstream of LPA_1-$G\alpha_i$ signaling might interfere with the RhoA-ROCK activation downstream of *mil*-$G\alpha_{12/13}$ signaling, leading to the cardiac cell migration defect and the two heart phenotype. Third, we speculate that endoderm cells are the cells in which the functional interaction occurs. It was reported that the endoderm cells that are associated with migrating cardiac cells expressed significant amount of *s1pr2/mil* mRNA (*15*, *27*). In addition, the endoderm cells are in the vicinity of yolk syncytial layer that expresses *spns2* and thus produces S1P (*16*). *Lpar1* and *s1pr2/mil* showed a similar expression pattern in the heart field of developing zebrafish embryos (*21*), supporting the hypothesis.

We also examined if endogenous LPA signaling down-regulates S1P signaling. However, the *mil* or *spns2* MO-induced cardia bifida phenotype was not rescued by *lpar1* MO or Ki16425 (data not shown), suggesting that endogenous LPA_1 signaling does not suppress the S1P signaling in zebrafish cardiac cell migration. Recently, several studies have indicated that excessive Atx-LPA_1 signaling leads to the development of several chronic diseases such as lung fibrosis and arthritis (*33–35*). It is interesting to examine if S1P signaling is suppressed in such diseases and up-regulation of S1P signaling leads to the treatment.

In conclusion, we found two opposite effects of LPA and S1P signaling in zebrafish cardiomyocyte migration. The present results raise the possibility that LPA signaling acts as a modulator of S1P signaling *in vivo*. Further analyses will be necessary to elucidate the precise molecular mechanism of the interaction between LPA and S1P signaling at the cellular level.

Supplementary Data

Supplementary Data are available at *JB* Online.

Funding

This study was supported by Grant in aid for Scientific Research from the Ministry of Education, Culture, Sports, Science, and Technology of Japan (to K.H., A.I. and J.A.), the National Institute of Biomedical Innovation (to J.A.), Japan Science and Technology Agency Precursory Research for Embryonic Science and Technology (PRESTO) (to A.I.), Core Research for Evolutional Science and Technology (CREST) (to J.A.).

Conflict of interest

None declared.

References

1. Tigyi, G. and Miledi, R. (1992) Lysophosphatidates bound to serum albumin activate membrane currents in Xenopus oocytes and neurite retraction in PC12 pheochromocytoma cells. *J. Biol. Chem.* **267**, 21360–21367
2. Sato, K., Malchinkhuu, E., Muraki, T., Ishikawa, K., Hayashi, K., Tosaka, M., Mochiduki, A., Inoue, K., Tomura, H., Mogi, C., Nochi, H., Tamoto, K., and Okajima, F. (2005) Identification of autotaxin as a neurite retraction-inducing factor of PC12 cells in cerebrospinal fluid and its possible sources. *J. Neurochem.* **92**, 904–914
3. Yatomi, Y., Igarashi, Y., Yang, L., Hisano, N., Qi, R., Asazuma, N., Satoh, K., Ozaki, Y., and Kume, S. (1997) Sphingosine 1-phosphate, a bioactive sphingolipid abundantly stored in platelets, is a normal constituent of human plasma and serum. *J. Biochem.* **121**, 969–973
4. Sato, K., Malchinkhuu, E., Horiuchi, Y., Mogi, C., Tomura, H., Tosaka, M., Yoshimoto, Y., Kuwabara, A., and Okajima, F. (2007) HDL-like lipoproteins in cerebrospinal fluid affect neural cell activity through lipoprotein-associated sphingosine 1-phosphate. *Biochem. Biophys. Res. Commun.* **359**, 649–654
5. Chun, J., Hla, T., Lynch, K.R., Spiegel, S., and Moolenaar, W.H. (2010) International Union of Basic and Clinical Pharmacology. LXXVIII. Lysophospholipid receptor nomenclature. *Pharmacol. Rev.* **62**, 579–587
6. Donati, C., Cencetti, F., and Bruni, P. (2013) New insights into the role of sphingosine 1-phosphate and lysophosphatidic acid in the regulation of skeletal muscle cell biology. *Biochim. Biophys. Acta* **1831**, 176–184
7. Tanaka, M., Okudaira, S., Kishi, Y., Ohkawa, R., Iseki, S., Ota, M., Noji, S., Yatomi, Y., Aoki, J., and Arai, H. (2006) Autotaxin stabilizes blood vessels and is required for embryonic vasculature by producing lysophosphatidic acid. *J. Biol. Chem.* **281**, 25822–25830
8. Liu, Y., Wada, R., Yamashita, T., Mi, Y., Deng, C.X., Hobson, J.P., Rosenfeldt, H.M., Nava, V.E., Chae, S.S., Lee, M.J., Liu, C.H., Hla, T., Spiegel, S., and Proia, R.L. (2000) Edg-1, the G protein-coupled receptor for sphingosine-1-phosphate, is essential for vascular maturation. *J. Clin. Invest.* **106**, 951–961
9. Sumida, H., Noguchi, K., Kihara, Y., Abe, M., Yanagida, K., Hamano, F., Sato, S., Tamaki, K., Morishita, Y., Kano, M.R., Iwata, C., Miyazono, K., Sakimura, K., Shimizu, T., and Ishii, S. (2010) LPA4 regulates blood and lymphatic vessel formation during mouse embryogenesis. *Blood* **116**, 5060–5070
10. Tokumura, A., Fukuzawa, K., and Tsukatani, H. (1978) Effects of synthetic and natural lysophosphatidic acids on the arterial blood pressure of different animal species. *Lipids* **13**, 572–574
11. Sugiyama, A., Yatomi, Y., Ozaki, Y., and Hashimoto, K. (2000) Sphingosine 1-phosphate induces sinus tachycardia and coronary vasoconstriction in the canine heart. *Cardiovasc. Res.* **46**, 119–125
12. Tokumura, A., Yotsumoto, T., Masuda, Y., and Tanaka, S. (1995) Vasopressor effect of lysophosphatidic acid on spontaneously hypertensive rats and Wistar Kyoto rats. *Res. Commun. Mol. Pathol. Pharmacol.* **90**, 96–102
13. Sanna, M.G., Liao, J., Jo, E., Alfonso, C., Ahn, M.Y., Peterson, M.S., Webb, B., Lefebvre, S., Chun, J., Gray, N., and Rosen, H. (2004) Sphingosine 1-phosphate (S1P) receptor subtypes S1P1 and S1P3, respectively, regulate lymphocyte recirculation and heart rate. *J. Biol. Chem.* **279**, 13839–13848
14. Yukiura, H., Hama, K., Nakanaga, K., Tanaka, M., Asaoka, Y., Okudaira, S., Arima, N., Inoue, A.,

Hashimoto, T., Arai, H., Kawahara, A., Nishina, H., and Aoki, J. (2011) Autotaxin regulates vascular development via multiple lysophosphatidic acid (LPA) receptors in zebrafish. *J. Biol. Chem.* **286**, 43972–43983

15. Kupperman, E., An, S., Osborne, N., Waldron, S., and Stainier, D.Y. (2000) A sphingosine-1-phosphate receptor regulates cell migration during vertebrate heart development. *Nature* **406**, 192–195
16. Kawahara, A., Nishi, T., Hisano, Y., Fukui, H., Yamaguchi, A., and Mochizuki, N. (2009) The sphingolipid transporter spns2 functions in migration of zebrafish myocardial precursors. *Science* **323**, 524–527
17. Osborne, N., Brand-Arzamendi, K., Ober, E.A., Jin, S.W., Verkade, H., Holtzman, N.G., Yelon, D., and Stainier, D.Y. (2008) The spinster homolog, two of hearts, is required for sphingosine 1-phosphate signaling in zebrafish. *Curr. Biol.* **18**, 1882–1888
18. Fukuhara, S., Simmons, S., Kawamura, S., Inoue, A., Orba, Y., Tokudome, T., Sunden, Y., Arai, Y., Moriwaki, K., Ishida, J., Uemura, A., Kiyonari, H., Abe, T., Fukamizu, A., Hirashima, M., Sawa, H., Aoki, J., Ishii, M., and Mochizuki, N. (2012) The sphingosine-1-phosphate transporter Spns2 expressed on endothelial cells regulates lymphocyte trafficking in mice. *J. Clin. Invest.* **122**, 1416–1426
19. Hisano, Y., Kobayashi, N., Yamaguchi, A., and Nishi, T. (2012) Mouse SPNS2 functions as a sphingosine-1-phosphate transporter in vascular endothelial cells. *PLoS One* **7**, e38941
20. Kimmel, C.B., Ballard, W.W., Kimmel, S.R., Ullmann, B., and Schilling, T.F. (1995) Stages of embryonic development of the zebrafish. *Dev. Dyn.* **203**, 253–310
21. Lee, S.J., Chan, T.H., Chen, T.C., Liao, B.K., Hwang, P.P., and Lee, H. (2008) LPA1 is essential for lymphatic vessel development in zebrafish. *FASEB J.* **22**, 3706–3715
22. Thisse, C. and Thisse, B. (2008) High-resolution in situ hybridization to whole-mount zebrafish embryos. *Nat. Protoc.* **3**, 59–69
23. Inoue, A., Arima, N., Ishiguro, J., Prestwich, G.D., Arai, H., and Aoki, J. (2011) LPA-producing enzyme PA-PLA$_1\alpha$ regulates hair follicle development by modulating EGFR signalling. *EMBO J.* **30**, 4248–4260
24. Inoue, A., Ishiguro, J., Kitamura, H., Arima, N., Okutani, M., Shuto, A., Higashiyama, S., Ohwada, T., Arai, H., Makide, K., and Aoki, J. (2012) TGFα shedding assay: an accurate and versatile method for detecting GPCR activation. *Nat. Methods* **9**, 1021–1029
25. Umezu-Goto, M., Kishi, Y., Taira, A., Hama, K., Dohmae, N., Takio, K., Yamori, T., Mills, G.B., Inoue, K., Aoki, J., and Arai, H. (2002) Autotaxin has lysophospholipase D activity leading to tumor cell growth and motility by lysophosphatidic acid production. *J. Cell Biol* **158**, 227–233
26. Sato, T., Sugimoto, K., Inoue, A., Okudaira, S., Aoki, J., and Tokuyama, H. (2012) Synthesis and biological evaluation of optically active Ki16425. *Bioorg. Med. Chem. Lett.* **22**, 4323–4326
27. Ye, D. and Lin, F. (2013) S1pr2/Gα13 signaling controls myocardial migration by regulating endoderm convergence. *Development* **140**, 789–799
28. Van Leeuwen, F.N., Olivo, C., Grivell, S., Giepmans, B.N., Collard, J.G., and Moolenaar, W.H. (2003) Rac activation by lysophosphatidic acid LPA1 receptors through the guanine nucleotide exchange factor Tiam1. *J. Biol. Chem.* **278**, 400–406
29. Leeuwen, F.N., Kain, H.E., Kammen, R.A., Michiels, F., Kranenburg, O.W., and Collard, J.G. (1997) The guanine nucleotide exchange factor Tiam1 affects neuronal morphology; opposing roles for the small GTPases Rac and Rho. *J. Cell Biol* **139**, 797–807
30. Sander, E.E., ten Klooster, J.P., van Delft, S., van der Kammen, R.A., and Collard, J.G. (1999) Rac downregulates Rho activity: reciprocal balance between both GTPases determines cellular morphology and migratory behavior. *J. Cell Biol* **147**, 1009–1022
31. Wei, L., Roberts, W., Wang, L., Yamada, M., Zhang, S., Zhao, Z., Rivkees, S.A., Schwartz, R.J., and Imanaka-Yoshida, K. (2001) Rho kinases play an obligatory role in vertebrate embryonic organogenesis. *Development* **128**, 2953–2962
32. Matsui, T., Raya, A., Kawakami, Y., Callol-Massot, C., Capdevila, J., Rodríguez-Esteban, C., and Izpisúa Belmonte, J.C. (2005) Noncanonical Wnt signaling regulates midline convergence of organ primordia during zebrafish development. *Genes Dev.* **19**, 164–175
33. Tager, A.M., LaCamera, P., Shea, B.S., Campanella, G.S., Selman, M., Zhao, Z., Polosukhin, V., Wain, J., Karimi-Shah, B.A., Kim, N.D., Hart, W.K., Pardo, A., Blackwell, T.S., Xu, Y., Chun, J., and Luster, A.D. (2008) The lysophosphatidic acid receptor LPA1 links pulmonary fibrosis to lung injury by mediating fibroblast recruitment and vascular leak. *Nat. Med.* **14**, 45–54
34. Oikonomou, N., Mouratis, M.A., Tzouvelekis, A., Kaffe, E., Valavanis, C., Vilaras, G., Karameris, A., Prestwich, G.D., Bouros, D., and Aidinis, V. (2012) Pulmonary autotaxin expression contributes to the pathogenesis of pulmonary fibrosis. *Am. J. Respir. Cell Mol. Biol.* **47**, 566–574
35. Nikitopoulou, I., Oikonomou, N., Karouzakis, E., Sevastou, I., Nikolaidou-Katsaridou, N., Zhao, Z., Mersinias, V., Armaka, M., Xu, Y., Masu, M., Mills, G.B., Gay, S., Kollias, G., and Aidinis, V. (2012) Autotaxin expression from synovial fibroblasts is essential for the pathogenesis of modeled arthritis. *J. Exp. Med.* **209**, 925–933

MCB
Journals.ASM.org

Screening with a Novel Cell-Based Assay for TAZ Activators Identifies a Compound That Enhances Myogenesis in C2C12 Cells and Facilitates Muscle Repair in a Muscle Injury Model

Zeyu Yang,[a,b] Kentaro Nakagawa,[a] Aradhan Sarkar,[a] Junichi Maruyama,[a] Hiroaki Iwasa,[a] Yijun Bao,[a,c] Mari Ishigami-Yuasa,[d] Shigeru Ito,[e] Hiroyuki Kagechika,[d,e] Shoji Hata,[f] Hiroshi Nishina,[f] Shinya Abe,[g] Masanobu Kitagawa,[g] Yutaka Hata[a,h]

Department of Medical Biochemistry, Graduate School of Medical and Dental Sciences, Tokyo Medical and Dental University, Tokyo, Japan[a]; Department of Ultrasound, Shengjing Hospital of China Medical University, Shenyang, China[b]; Department of Neurosurgery, First Hospital of China Medical University, Shenyang, China[c]; Chemical Biology Screening Center[d] and Institute of Biomaterials and Bioengineering,[e] Tokyo Medical and Dental University, Tokyo, Japan; Department of Developmental and Regenerative Biology, Medical Research Institute, Tokyo Medical and Dental University, Tokyo, Japan[f]; Department of Comprehensive Pathology, Graduate School of Medical and Dental Sciences, Tokyo Medical and Dental University, Tokyo, Japan[g]; Center for Brain Integration Research, Tokyo Medical and Dental University, Tokyo, Japan[h]

The transcriptional coactivator with a PDZ-binding motif (TAZ) cooperates with various transcriptional factors and plays various roles. Immortalized human mammalian epithelial MCF10A cells form spheres when TAZ is overexpressed and activated. We developed a cell-based assay using sphere formation by TAZ-expressing MCF10A cells as a readout to screen 18,458 chemical compounds for TAZ activators. Fifty compounds were obtained, and 47 were confirmed to activate the TAZ-dependent TEAD-responsive reporter activity in HEK293 cells. We used the derived subset of compounds as a TAZ activator candidate minilibrary and searched for compounds that promote myogenesis in mouse C2C12 myoblast cells. In this study, we focused on one compound, IBS008738. IBS008738 stabilizes TAZ, increases the unphosphorylated TAZ level, enhances the association of MyoD with the myogenin promoter, upregulates MyoD-dependent gene transcription, and competes with myostatin in C2C12 cells. TAZ knockdown verifies that the effect of IBS008738 depends on endogenous TAZ in C2C12 cells. IBS008738 facilitates muscle repair in cardiotoxin-induced muscle injury and prevents dexamethasone-induced muscle atrophy. Thus, this cell-based assay is useful to identify TAZ activators with a variety of cellular outputs. Our findings also support the idea that TAZ is a potential therapeutic target for muscle atrophy.

The transcriptional coactivator with a PDZ-binding motif (TAZ, also called WWTR1) was identified as a 14-3-3-binding protein (1–3). It is similar to Yes-associated protein 1 (YAP1) in its molecular structure, which consists of an N-terminal TEAD-binding domain, one or two WW domains, and a transcriptional activation domain (4). The Hippo pathway is a tumor suppressor signaling pathway that was initially identified in *Drosophila* (2, 5, 6). TAZ is phosphorylated at four sites by large tumor suppressor kinase 1 (LATS1) and LATS2, which are core kinases of the Hippo pathway (1–3). Phosphorylated TAZ is trapped by 14-3-3, is recruited from the nucleus to the cytoplasm, and undergoes protein degradation (1–3). In this way, the Hippo pathway negatively regulates TAZ. In addition to the Hippo pathway, TAZ is regulated by cell junction proteins such as ZO-1, ZO-2, and angiomotin (7–10). Recent studies have revealed that TAZ is under the control of the actin cytoskeleton and the mechanical stretch (11–13). Moreover, Wnt signaling stabilizes TAZ (14–16). Conversely, cytoplasmic TAZ binds β-catenin and Dishevelled (DVL) and inhibits β-catenin nuclear localization and DVL phosphorylation to negatively regulate the Wnt pathway. This shows that TAZ plays a pivotal role in the cross talk between the Hippo pathway and the Wnt pathway.

In human cancers, the Hippo pathway is frequently compromised, resulting in TAZ hyperactivity (6). TAZ gene amplification is also detected in cancers (17–21). TAZ hyperactivity causes epithelial-mesenchymal transitions (EMT) and provides cancer cells with stemness (22–26). Hence, TAZ is considered a potential cancer therapeutic target. The transforming ability of TAZ is attributed mostly to the interaction with TEAD and Wbp2 (22, 27–29). Besides TEAD and Wbp2, TAZ interacts with numerous transcriptional factors. TAZ interacts with thyroid transcription factor 1, Pax8, and T-box transcription factor 5 and is important for lung, thyroid, heart, and limb development (30, 31). It also interacts with p300 (31). In human embryonic stem cells, TAZ interacts with SMAD2, -3, and -4 and is essential for the maintenance of self-renewal (16, 32, 33). In mesenchymal stem cells, TAZ interacts with peroxisome proliferator-activated receptor γ and Runx2 to suppress adipogenesis and promote osteogenesis (34, 35). In skeletal muscles, TAZ interacts with transcriptional factors that are implicated in myogenesis. It binds the key myogenic regulators Pax3 and MyoD (36, 37). TEAD binds to the so-called MCAT elements (muscle C, A, and T; 5′-CATTCC-3′) in muscle-specific genes such as that for myogenin (38). Although SMAD2 and -3, which are TAZ interactors, mediate the inhibitory signal of myostatin in muscle cells (39), TAZ is overall regarded as a myogenesis-promoting factor. This makes a sharp contrast with YAP1, whose activation induces muscle atrophy (40, 41).

Received 8 October 2013 **Returned for modification** 31 October 2013
Accepted 11 February 2014
Published ahead of print 18 February 2014
Address correspondence to Yutaka Hata, yuhammch@tmd.ac.jp.
Supplemental material for this article may be found at http://dx.doi.org/10.1128/MCB.01346-13.

doi:10.1128/MCB.01346-13

Sarcopenia is a skeletal muscle atrophy associated with ageing (42). Sarcopenia deprives elderly populations of the ability to live independently and will be a major health concern in industrialized countries. Appropriate exercise and nutrition are key factors in the prevention and treatment of sarcopenia. However, the development of drugs to increase skeletal muscles is also required. Satellite cells are considered skeletal muscle progenitor cells and a major source to regenerate muscle tissue in adults. Although the role of TAZ in the maintenance of muscle satellite cells remains to be clarified, considering the potential role of TAZ in myogenesis, we expected that TAZ activators are beneficial for the therapy of sarcopenia. We established a cell-based assay for TAZ activators, screened 18,458 chemical compounds, and obtained 50 TAZ activator candidates. We subsequently selected compounds that promote myogenesis in mouse C2C12 myoblast cells and finally focused on one compound that facilitates muscle repair in an injury model and prevents dexamethasone-induced muscle atrophy.

MATERIALS AND METHODS

DNA constructs and virus production. The pLenti-EF-ires-blast, pClneoFH, and pClneoHA vectors were described previously (43–45). A TAZ SA mutant, in which serine 89 is mutated to alanine, was prepared by the PCR method. pLenti-EF-FH-TAZ and TAZ SA-ires-blast were prepared by subcloning NheI/SalI fragments from pClneoFH-TAZ and pClneoFH-TAZ S89A into the pLenti-EF-ires-blast vector. The BLOCK-iT Pol II miR RNA interference (RNAi) expression vector kit (Invitrogen) was used to generate pcDNA knockdown constructs for human LATS1 and LATS2. The target sequences were a 1,074-bp site of LATS1 (AF104413.1) and a 1,598-bp site of LATS2 (AF207547.1). The annealing oligonucleotides were ligated into the pcDNA 6.2-GW/miR vector according to the manufacturer's protocol to generate pcDNA 6.2 LATS1 KD and pcDNA 6.2 LATS2 KD. A BamHI/XhoI fragment was isolated from pcDNA 6.2 LATS2 KD and ligated into the BglII/XhoI sites of pcDNA 6.2 LATS1 KD to generate pcDNA 6.2 LATS1/2 KD. PCR was performed on pBudCE with primers H1674 (5′-ATCGATGTCGAGCTAGCTTCGTGAG-3′) and H1675 (5′-ACTAGTCTCGAGACCACGTGTTCACGACACC-3′) to amplify the elongation factor (EF) promoter. The PCR product was digested with ClaI and SpeI and ligated into the same sites of pLenti4/TO/V5-DEST to replace the pCMV/VO promoter with the EF promoter and to generate pLenti4-EF/V5-DEST. The pLenti-EmGFP LATS1/2 KD vector was generated by using the ViraPower T-REx lentiviral expression system from pcDNA 6.2 LATS1/2 KD and pLenti4-EF/V5-DEST. The NheI/NotI fragment from pBudCE4.1 was ligated into the XbaI/NotI sites of pQCXIP (Clontech) to generate pQCXIP EF. The linker (H3142 [5′-GGCCGCTCGAGTTTAAACAATTGGATCC-3′] and H-3143 [5′-AATTGGATCCAATTGTTTAAACTCGAGC-3′]) was subcloned into the NotI/EcoRI sites to generate pQCXIP EF H3142/H3143. The BglII/NotI fragment from pClneo mCherry was ligated into the BglII/NotI sites of pQCXIP EF H3142/H3143 to generate pQCXIP mCherry, which was digested with BamHI/EcoRV, filled in, and religated to remove the internal ribosome entry sites and the puromycin resistance gene. The resulting vector was named pQCXI mCherry. pLenti-siRNA-GFP (Applied Biological Materials Inc.) was digested with SpeI/MluI. The isolated green fluorescent protein (GFP)-2A-puro fragment was subcloned into NheI/MluI sites of pClneo to generate pClneo GFP-2A-puro, which was subsequently digested with BglII/MluI. The isolated fragment was ligated into the BglII/MluI sites of pQCXI mCherry to generate pQCXI GFP2A-puromycin. WWTR1 mouse pRFP-RS short hairpin RNA (shRNA) (TF505533, 561750; OriGene) was purchased, and PCR was performed with primers H3163 (5′-CAATTGAATTCCCCAGTGGAAAGACGCGCA-3′) and H3164 (5′-ACGCGTCTCGAGCCTGGGGACTTTCACAC-3′) to amplify the U6 promoter and the target sequence. The PCR product was subcloned into the TAKN2 vector (BioDynamics Laboratory Inc.) and digested with MluI/NotI. The isolated fragment was ligated into the MluI/NotI sites of pQCXI GFP2A-puromycin. The vector was cotransfected with the pCL10A-1 retrovirus packaging vector into HEK293 cells to generate retrovirus for mouse TAZ knockdown. Lentivirus was generated as described previously (46).

Antibodies and reagents. The rat anti-YAP monoclonal antibody used was described previously (43). The following antibodies and reagents were obtained from commercial sources. The mouse anti-TAZ (560235), mouse anti-MyoD (554130), mouse anti-poly(ADP-ribose) polymerase (anti-PARP) (51-6639GR), mouse antifibronectin (610077), mouse anti-E-cadherin (610181), and mouse anti-N-cadherin (610921) antibodies and Matrigel were from BD Pharmingen. The rabbit antimyogenin (sc-576), rabbit anti-MyoD (sc-760), and mouse antivimentin (sc-6260) antibodies were from Santa Cruz. The mouse anti-myosin heavy chain (anti-MHC) (MF20), mouse anti-Pax7, and mouse anti-Pax3 antibodies were from the Developmental Studies Hybridoma Bank, University of Iowa. The rabbit antilaminin (L9293), mouse anti-α-tubulin (T9026), and mouse anti-FLAG M2 (F3165) antibodies; Hoechst 33342; *Naja mossambica* cardiotoxin; dexamethasone (C9759); epidermal growth factor (E9644); insulin (I5500), and 3-(4,5-dimethylthiazol-2-yl)-2,5-diphenyltetrazolium bromide (MTT) were from Sigma-Aldrich. Basic fibroblast growth factor (064-04541) and Phos-tag acrylamide were from Wako Chemicals. The mouse antimyogenin antibody (ab1835) was from Abcam. The mouse antihemagglutinin (anti-HA) antibody was from Roche. The mouse antiactin (clone 4) and mouse antipuromycin (clone 12D10) antibodies were from Millipore. The rabbit anti-TEAD4 antibody (APR38726_P050) was from Aviva. The goat anti-Pax3 antibody (GWB-3AE0a5) was from Genway Biotech Inc. The recombinant myostatin (788-G8-010) was from R&D Systems.

Cell culture and transfection. HEK293, A431, and HCT116 cells were cultured in Dulbecco's modified Eagle medium (DMEM) containing 10% fetal bovine serum (FBS) and 10 mM HEPES-NaOH at pH 7.4 under 5% CO_2 at 37°C. MCF10A cells were cultured in DMEM–F-12 supplemented with 5% horse serum (Invitrogen), 20 ng/ml epidermal growth factor, 0.5 μg/ml hydrocortisone, and 10 μg/ml insulin. DNA transfection was performed with Lipofectamine 2000 (Invitrogen). MCF10A-TAZ and MCF10A-TAZ SA cells were prepared with pLenti-EF-FH-TAZ-ires-blast and pLenti-EF-FH-TAZ SA-ires-blast lentivirus vectors with blasticidin selection. C2C12 cells were passaged in growth medium (DMEM containing 10% FBS) and differentiated in C2C12 differentiation medium containing DMEM and 2% horse serum (Invitrogen). C2C12 cells in which TAZ was stably knocked down were prepared with pQCXI-GFP-2A-sh mouse TAZ retrovirus. To stably knock down LATS1 and LATS2 in MCF10A-TAZ cells, the cells were infected with pLenti-EmGFP-LATS1/2 KD lentivirus and GFP-positive cells were collected by fluorescence-activated cell sorting.

Quantitative RT-PCR. Quantitative RT-PCR analysis was performed with SYBR green (Roche) and the ABI7500 real-time PCR system (Applied Biosystems) (44). For the primers used, see Table S1 in the supplemental material.

RNAi. Human TAZ and mouse TAZ were knocked down in MCF10A and C2C12 cells as described previously (44). The double-stranded RNAs (dsRNAs) used were human TAZ s24789 (Ambion) and mouse TAZ siRNA D-041057 (Dharmacon). Knockdown was confirmed by quantitative RT-PCR or immunoblotting.

Myofusion index. C2C12 cells were fixed and immunostained with anti-MHC antibody. Nuclei were visualized with Hoechst 33342. The fusion index was calculated as a percentage of the nuclei detected within MHC-positive multinuclear cells.

Reporter assay. The TEAD reporter assay was performed with HEK293 cells as described previously (43). C2C12 cells were plated at 1×10^5/well in 12-well plates and cultured overnight. The cells were transfected with the pGL3 Myo-184 (MyoD), 8×GT-IIC-δ51LucII (for TEAD), 9×CAGA-MLP (for SMAD), and $p(PRS\text{-}1/\text{-}4)_3$ (for Pax3) luciferase reporter vectors alone or with TAZ. These reporter vectors were from Kenji Miyazawa (Yamanashi University), Hiroshi Sasaki (Ku-

mamoto University), and Hiroki Kurihara (The University of Tokyo) (37, 47, 48). Dimethyl sulfoxide (DMSO) or 10 μM IBS008738 was added 6 h after transfection. The cells were grown to confluence, transferred to differentiation medium with DMSO or 10 μM IBS008738, and cultured for 24 h before luciferase assays were performed.

ChIP analysis. Chromatin immunoprecipitation (ChIP) experiments were based on the protocol described by Nelson et al. (49). In brief, C2C12 myoblasts were cultured to confluence and then treated with DMSO or 10 μM IBS008738 in differentiation medium for 24 h. Cells were cross-linked in 1.42% (vol/vol) formaldehyde for 15 min, and the reaction was quenched for 5 min with 125 mM glycine. Cross-linked cells were lysed in buffer (50 mM Tris-HCl [pH 7.5], 150 mM NaCl, 5 mM EDTA, 0.5% [vol/vol] Nonidet P-40, 1% [vol/vol] Triton X-100), and chromatin was sheared by 25 consecutive rounds in a sonicator bath (Bioruptor; Diagenode) at maximum output and cycles of 30 s on and 60 s off. Shearing was analyzed by agarose gel electrophoresis. Chromatin from about 2×10^6 cells was incubated for 3 h at 4°C with 2 μg of antibodies. Immunoprecipitation was done with 20 μl of protein G-Sepharose beads. Protein G-Sepharose without antibody was used as the control (mock ChIP). The immunoprecipitated DNA fragments were isolated with Chelex-100 resin and diluted 1:2.5 for quantitative PCR analysis. Input-normalized relative abundance was determined. For the sequences of the primers used, see Table S1 in the supplemental material.

Subcellular fractionation. Subcellular fractionation was performed as described previously (43).

Myostatin inhibition assay. C2C12 cells were transfected with control or TAZ dsRNA. Forty-eight hours later, the cells were plated in growth medium at 2×10^5/well in 12-well plates. When grown to confluence, the cells were transferred to differentiation medium with DMSO, 100 ng/ml myostatin, 10 μM IBS008738, or a combination of myostatin and IBS008738 and cultured for 3 days. The differentiation medium containing the reagents was changed every day.

Cell proliferation and viability assessment. Cell proliferation and viability were assessed by MTT formazan dye conversion.

Sphere formation assay and 3D Matrigel culture. MCF10A and A431 cells were plated at 300/well in 96-well Ultra Low Attachment plates (Corning) and cultured for 10 days in serum-free DMEM–F-12 (Invitrogen) containing 10 ng/ml basic fibroblast growth factor, 20 ng/ml epidermal growth factor, 5 μg/ml insulin, and 0.4% (wt/vol) bovine serum albumin. A cell aggregate with a diameter of more than 150 μm was defined as a sphere. For three-dimensional (3D) Matrigel culture, 96-well plates were precoated with 30 μl of Matrigel per well. Cells were suspended at 2.1×10^6/liter in medium containing 2% Matrigel. Cell suspension volumes of 140 μl containing 300 cells were plated into each well and cultured for 10 days with DMSO or 10 μM IBS008738.

Animals. All experimental procedures were approved by the Institutional Animal Care and Use Committee. Six-week-old female BALB/cByJ mice (Clea Japan Inc.) were used. *N. mossambica* cardiotoxin was dissolved in phosphate-buffered saline (PBS) at a final concentration of 10 μM. A 100-μl volume of cardiotoxin solution was injected with either control DMSO or 3 nmol of IBS008738 (0.3 μl of DMSO or 0.3 μl of 10 mM IBS008738 was diluted in 100 μl of PBS) into the tibialis anterior (TA) muscle of mice ($n = 6$) under anesthesia. Mice were sacrificed on days 2, 5, 7, and 14. For dexamethasone-induced muscle atrophy, dexamethasone (25 mg/kg/day) or DMSO was injected intraperitoneally from day 1 to day 7. A 100-μl volume of 30 μM IBS008738 or DMSO in PBS was injected into the TA and gastrocnemius (GM) muscles on days 9, 11, and 13. Mice were sacrificed on day 14.

Skeletal muscle histology. TA and GM muscles were fixed in 4% formalin and embedded in paraffin. Muscle sections 5 μm thick were stained with hematoxylin and eosin. For the immunostaining of Pax7, MyoD, and laminin, 10-μm frozen sections were fixed with acetone at −20°C for 10 min, incubated with primary antibodies at 4°C overnight, and then visualized with secondary antibodies. To quantify the extent of muscle regeneration, four sections of each muscle at 100-μm intervals were analyzed and the total number of centrally nucleated myofibers per visual field was determined manually. To assess muscle atrophy, muscles were sectioned at a 10-μm thickness and immunostained with anti-laminin antibody. The cross-sectional areas of myofibers were analyzed by using the ImageJ software.

Phosphate affinity SDS-PAGE. Phosphate affinity SDS-PAGE was performed with Phos-tag acrylamide (Wako Chemicals) and polyvinylidene difluoride (PVDF) membranes.

***In vivo* SUnSET technique.** *In vivo* SUnSET was used according to the previously reported protocol (50). Briefly, mice were anesthetized and intraperitoneally injected with 0.04 μmol/g puromycin in 100 μl of PBS. Thirty minutes later, GM muscles were removed and frozen in liquid N_2. Frozen tissues were homogenized in buffer containing 40 mM Tris-HCl at pH 7.5, 0.5% (wt/vol) Triton X-100, 1 mM EDTA, 5 mM EGTA, 25 mM β-glycerophosphate, 25 mM NaF, 1 mM Na_3VO_4, 10 mg/liter leupeptin, and 1 mM phenylmethylsulfonyl fluoride. Sixty-microgram samples of total proteins were analyzed by SDS-PAGE, and immunoblotting with antipuromycin antibody was performed with PVDF membranes. The membranes were stained with Coomassie brilliant blue.

Statistical analysis. Statistical analyses were performed with Student's *t* test for the comparison of two samples and analysis of variance with Dunnett's test for multiple comparisons with GraphPad Prism 5.0 (GraphPad Software).

Other procedures. Immunoprecipitation and immunofluorescence assay were performed as described previously (51).

RESULTS

Cell-based assay to screen for the chemical compounds that activate TAZ. We used immortalized human mammary epithelial MCF10A cells to screen for TAZ activators. LATS1- and LATS2-dependent phosphorylation at serine 89 is the key event in the regulation of TAZ. Neither parent MCF10A cells nor MCF10A cells expressing TAZ (MCF10A-TAZ) survive under mammosphere-forming conditions, while MCF10A cells expressing S89A mutant TAZ (MCF10A-TAZ SA) do form spheres (Fig. 1A). However, with LATS1 and LATS2 knockdown, MCF10A-TAZ cells, but not parent MCF10A cells, form spheres (Fig. 1B). The additional knockdown of TAZ abolished the effect of LATS1 and LATS2 knockdown in MCF10A-TAZ cells (Fig. 1C and D). These findings indicate that sphere formation by MCF10A-TAZ cells reflects the activity of overexpressed TAZ.

The screening of 18,458 chemical compounds yielded 50 TAZ activator candidates. We cultured MCF10A-TAZ cells under sphere-forming conditions with 18,458 chemical compounds at 10 μM for 14 days. Fifty compounds enabled MCF10A-TAZ cells to form spheres (we defined a cell aggregate with a longest diameter of >150 μm as a sphere). We next performed the TEAD reporter assay with these 50 compounds. Forty-seven compounds enhanced TAZ-dependent TEAD reporter activity (data not shown).

TAZ activators enhanced myogenesis in C2C12 cells. TAZ plays important roles in the regulation of osteogenesis, adipogenesis, and myogenesis (34, 52). Here we focused on myogenesis and applied 50 compounds to mouse C2C12 myoblast cells. C2C12 cells were cultured under growth conditions. After grown to confluence, the cells were switched to differentiation conditions and cultured for 72 h in differentiation medium containing 10 μM each compound. We evaluated myogenesis by determining the myofusion index (the number of nuclei detected in multinuclear MHC-positive cells divided by the total number of nuclei). Cells treated with 43 compounds exhibited higher myogenesis than control cells (data not shown). In this study, we focused on one